NASA-CR-199668

ORIGINAL CONTAINS
COLOR ILLUSTRATIONS
4

NAGW-4336
INTERIM
IN-54-CR
5667
P-79

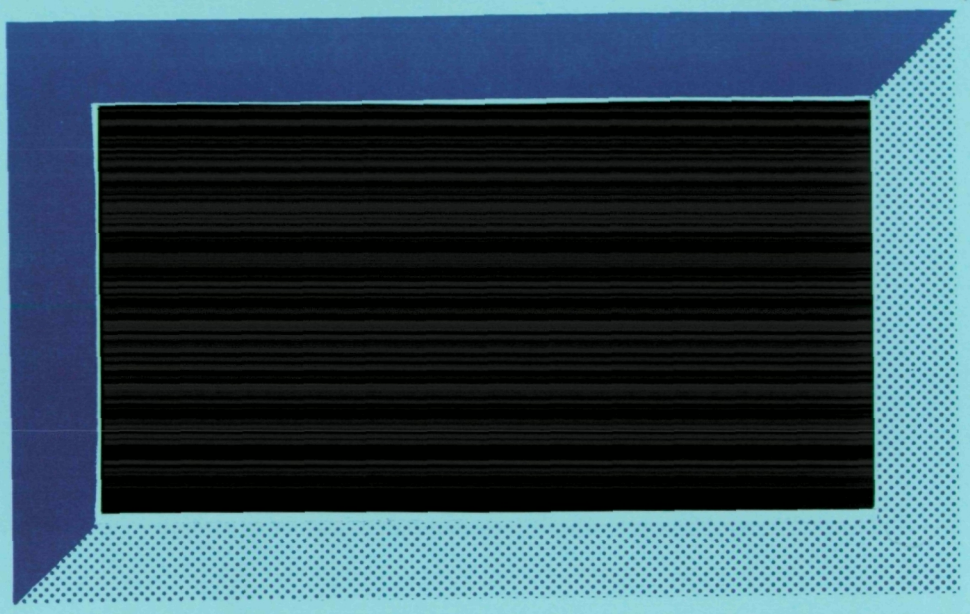

(NASA-CR-199668) DYNAMIC ANALYSIS OF ASTRONAUT MOTIONS IN MICROGRAVITY: APPLICATIONS FOR EXTRAVEHICULAR ACTIVITY (EVA) Annual Report (MIT) 79 p

N96-13451

Unclas

G3/54 0073766

DEPARTMENT OF
AERONAUTICS AND ASTRONAUTICS
MASSACHUSETTS INSTITUTE OF TECHNOLOGY
CAMBRIDGE, MASSACHUSETTS 02139

Dynamic Analysis of Astronaut Motions in Microgravity:
Applications for Extravehicular Activity (EVA)

PI: Prof. Dava J. Newman
Dept. of Aeronautics and Astronautics
MIT, 33-119
77 Massachusetts Ave.
Cambridge, MA 02139

Grant. Schaffner, MIT, Graduate Research Assistant

Annual Status Report for "Data-Driven Models to Describe Astronaut Performance in Microgravity: Full-Body Dynamics and Postural Control" under NASA Grant NAGW-4336.

Distribution:
Dr. Ronald White, NASA Technical Monitor
NASA Headquarters
UL/Life&Biomedical Sciences and Applications Division
300 E. Street, SW
Washington, D.C. 20546
(202) 358-2147

Mr. Calvin Mitchell
NASA Headquarters, MS: CWC
300 E Street, SW
Washington, D.C. 20546
(202) 358-0412

NASA Center for AeroSpace Information
P.O. Box 8757
Baltimore/Washington International Airport, Maryland 21240

DYNAMIC ANALYSIS OF ASTRONAUT MOTIONS DURING EXTRAVEHICULAR ACTIVITY

PI: Prof. Dava J. Newman
Dept. of Aeronautics and Astronautics
MIT, 33-119
77 Massachusetts Ave.
Cambridge, MA 02139

Grant. Schaffner, MIT, Graduate Research Assistant

Annual Status Report for "Data-Driven Models to Describe Astronaut Performance in Microgravity: Full-Body Dynamics and Postural Control" under NASA Grant NAGW-4336.
NASA Technical Monitor: Dr. Ronald White, NASA HQ, Code UL

Abstract

Simulations of astronaut motions during extravehicular activity (EVA) tasks were performed using computational multibody dynamics methods. The application of computational dynamic simulation to EVA was prompted by the realization that physical microgravity simulators have inherent limitations: viscosity in neutral buoyancy tanks; friction in air bearing floors; short duration for parabolic aircraft; and inertia and friction in suspension mechanisms. These limitations can mask critical dynamic effects that later cause problems during actual EVAs performed in space.

Methods of formulating dynamic equations of motion for multibody systems are discussed with emphasis on Kane's method, which forms the basis of the simulations presented herein. Formulation of the equations of motion for a two degree of freedom arm is presented as an explicit example. The four basic steps in creating the computational simulations were: *system description*, in which the geometry, mass properties, and interconnection of system bodies are input to the computer; *equation formulation* based on the system description; *inverse kinematics*, in which the angles, velocities, and accelerations of joints are calculated for prescribed motion of the endpoint (hand) of the arm; and *inverse dynamics*, in which joint torques are calculated for a prescribed motion. A graphical animation and data plotting program, EVADS (EVA Dynamics Simulation), was developed and used to analyze the results of the simulations that were performed on a Silicon Graphics Indigo2 computer.

EVA tasks involving manipulation of the Spartan 204 free flying astronomy payload, as performed during Space Shuttle mission STS-63 (February 1995), served as the subject for two dynamic simulations. An EVA crewmember was modeled as a seven segment system with an eighth segment representing the massive payload attached to the hand. For both simulations, the initial configuration of the lower body (trunk, upper leg, and lower leg) was a neutral microgravity posture. In the first simulation, the payload was manipulated around a circular trajectory of 0.15 m radius in 10 seconds. It was found that the wrist joint theoretically exceeded its ulnal deviation limit by as much as 49.8° and was required to exert torques as high as 26 N-m to accomplish the task, well in excess of the wrist physiological limit of 12 N-m. The largest torque in the first simulation, 52 N-m, occurred in the ankle joint. To avoid these problems, the second simulation placed the arm in a more comfortable initial position and the radius and speed of the circular trajectory were reduced by half. As a result, the joint angles and torques were reduced to values well within their physiological limits. In particular, the maximum wrist torque for the second simulation was only 3 N-m and the maximum ankle torque was only 6 N-m.

Table of Contents

List of Figures

List of Tables

List of Acronyms and Abbreviations

c.m.	center of mass
d.o.f.	degree(s) of freedom
EMU	Extravehicular Mobility Unit (Shuttle Spacesuit)
EVA	Extravehicular Activity
EVADS	EVA Dynamic Simulation
g	acceleration of free fall on Earth (9.806 m/s^2)
JSC	Johnson Space Center
MIT	Massachusetts Institute of Technology
NASA	National Aeronautics and Space Administration
PFR	Portable Foot Restraint
RMS	Remote Manipulator System
rpm	revolution(s) per minute
STS	Space Transportation System

1. Introduction

By way of introduction, this first chapter familiarizes the reader with the concept of extravehicular activity performed in spaceflight, the motivation for applying multibody dynamical simulation to extravehicular activity, and the objectives and contribution of the research effort. The chapter concludes with a synopsis of the contents of the report.

1.1 Objectives and Contribution

The primary objective of the research described in this report is to demonstrate the significant value of multibody dynamics analysis for the simulation of EVA tasks. In particular, it is believed that computational dynamic simulation has certain advantages over physical simulators and complements them very well. The main advantage is the ability to represent all the degrees of freedom available to a body in weightlessness (six degrees of freedom for a single isolated body - three translational and three rotational) and at the same time avoid some of the detrimental effects that physical simulators are subject to, such as friction in air bearing floors or viscous drag in neutral buoyancy facilities. Other advantages include low cost, flexibility, quick turnaround, low manpower requirements, and ease of operation.

Of course there is a price to pay for all these advantages. Simulation of multibody dynamics is inherently computationally intensive. In addition, greater accuracy and realism is gained through adding degrees of freedom and geometric detail to the dynamic system model, further increasing the complexity of the simulation, the computer processing time, and the work required of the analyst. In practice, the analyst must consider a tradeoff between the complexity of the dynamic system model and the accuracy and validity of the results in regards to the particular situation being simulated.

Certain specific objectives were established to guide the research effort. These 8 prioritized objectives are:

1) Develop a convenient means of modeling the dynamic system and tailor it to the particular needs of EVA simulation.

2) Transform the description of the dynamic system into equations of motion represented in computational form.

3) Develop computer code to drive simulations of the dynamic system under a variety of conditions.

4) Explore methods of prescribing the motions to be performed in a task-oriented form, the way that an astronaut or trainer might think of the operation, without the need to explicitly specify the kinematics (positions, velocities, and accelerations) of each segment. In other words, perform an inverse kinematics analysis, given only the motion of the endpoint of the system.

5) Determine the joint torques required to drive the system in performing a particular motion by using the calculated segment kinematics in an inverse dynamics analysis.

6) Create a graphical animation and data display user interface.

7) Show how the results of the inverse kinematics and inverse dynamics analyses are interpreted.

8) Demonstrate the means by which simulations are improved in an evolutionary manner.

To achieve these objectives a seven segment model of an astronaut is created with an eighth segment attached to the hand representing a large mass to be manipulated during an EVA task. The equations of motion are derived using SD/FAST, based on Kane's method, which creates code to represent the equations of motion in computational form. Additional code is created to drive the system during two simulations, the second simulation being an improvement on the first. Finally, the results are visualized through the aid of an animation and data plotting program, which has been named EVADS (EVA Dynamic Simulation). All of these operations are performed on a Silicon Graphics Indigo2 computer.

1.2 Synopsis of Report

In addition to the introduction chapter presented here, this report is comprised of chapters dealing with background information, methodology, results, and discussion and conclusions. The Background chapter provides a brief history of EVA; a description of

the space environment encountered in EVA (mostly in low Earth orbit); a summary of spacesuit requirements and the effects of the spacesuit's construction on human body dynamics; a discussion of training methods and physical simulators used in preparation for EVA; an introduction to computational simulation of multibody dynamics; and an example of dynamical simulation as applied to the modeling of the Intelsat VI satellite capture EVA.

The Methodology chapter first works through an example of dynamical equation formulation applied to a simple two degree of freedom system; then describes the Space Shuttle mission STS-63 Spartan mass handling EVA which serves as the subject for the two main simulations presented in the report; and finally presents the details of how the dynamic simulations are performed, including the creation of the system's description file, formulation of the equations of motion, inverse kinematics, inverse dynamics, and animation and data plots using EVADS. In both simulations, the EVA task is to manipulate the Spartan payload around a circular trajectory. In the first simulation, the radius of the circle is 0.15m and the trajectory is completed in 10 seconds. In the second simulation, the radius of the circle is 0.075m and the trajectory is completed in 20 seconds. In addition, the lower body joints (ankle, knee, and hip) are fixed in the first simulation, but are allowed some compliance (by means of passive springs and dampers) in the second simulation.

The Results chapter first presents data obtained from joint torque test functions, followed by data obtained from the two EVA simulations. It is observed that, in the first simulation, the wrist joint exceeds the range of motion limits and is required to exert torques beyond the level of human capability. The second simulation solves these problems by starting with the arm in a more comfortable position and by requiring the hand to follow a smaller circular trajectory at a lower speed (thus requiring less torque). The chapter concludes by presenting results of the animation and data plotting functions of EVADS.

In the Discussion and Conclusion chapter, the research objectives are recapped and the extent to which they were achieved is indicated. The results of the two simulations are deliberated with particular attention given to the success of implementing compliance in the lower body joints. The effectiveness of the animation and data representation abilities of EVADS is assessed. Some general conclusions about the research are drawn, especially relating to the feasibility of using computational multibody dynamics to simulate EVA tasks. Finally, the chapter concludes with suggestions for further research and a short summary of the report.

2. Methodology

This chapter describes how computational multibody dynamics can be applied to the analysis and simulation of EVA tasks. The first goal is to familiarize the reader with the process of multibody dynamical equation formulation and to demonstrate the complexity of these equations. A detailed example of this process as formulated by hand for a relatively simple system presents the equations in an explicit form. For clarity and convenience, the Lagrangian method is used for this first example. The remainder of the chapter describes how computational methods are employed to create computer simulations of more complex systems. The main steps are: the creation of a system description file; employing SD/FAST to derive the dynamical equations and simplify them using symbolic manipulation; development of user-written simulation driver code; and analysis of results by means of animation and plots. To illustrate these steps, a particular simulation example is presented based on an actual EVA mass handling task recently performed in space. In this case, the equations of motion are highly complex and would take several pages to write out. This would be extremely tedious to perform and would defeat the purpose of representing the equations implicitly by means of computer code and performing the analysis by numerical means. This chapter focuses on explaining how the system description file is created and how the simulation and analysis is carried out, while the interim step of generating the equations of motion is the domain of the commercially available program SD/FAST. Some general points on the SD/FAST computations were presented in the previous chapter. For more details on how the equations of motion are formulated, the reader is referred to additional references (Hollars, Rosenthal et al. 1994) (Kane, Likins et al. 1983) (Kane and Levinson 1985) (Rosenthal and Sherman 1986).

2.1 Example of Dynamical Equation Formulation

A relatively simple multibody system example has been chosen to ensure readability. The example is a two-body, two-d.o.f model of an astronaut's arm performing a manipulation task. It has been assumed that the rest of the astronaut's body has no influence on the dynamics of his arm motions because his torso is fixed in inertial space. As highly simplified as the scenario sounds, there is a conceivable situation in which the astronaut's backpack is affixed to an object with a much larger mass, such as the Space Shuttle Orbiter. The inertia of such a massive object would constrain the accelerations of

the astronaut's trunk to insignificant values allowing one to make the approximation that the trunk is stationary in inertial space. To further simplify the model, the arm is restricted to planar motion and only has two degrees of freedom: shoulder planar rotation and elbow joint extension and flexion. The upper and lower arm are modeled as rigid segments with constant moments of inertia. The hand is considered to be attached to the center of gravity of the object being manipulated. This model is sketched in Figure 2.1.

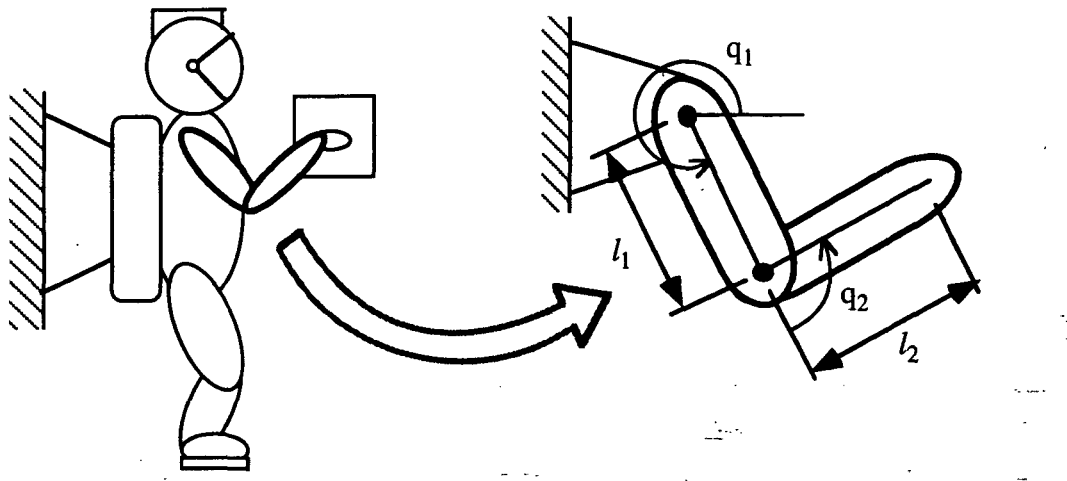

Figure 2.1 Two d.o.f. model of astronaut arm

As mentioned previously, the two most common classical formulations of multibody dynamics are the Newton-Euler formulation and the Lagrangian formulation. This astronaut arm motion example derives the equations of motion by means of the Lagrangian formulation in which the behavior of a dynamic system is described in terms of work and energy stored in the system. The advantage of the Lagrangian approach is that the constraint forces involved in the system are automatically eliminated, as opposed to the manual elimination required in the Newton-Euler method. Furthermore, the closed-form dynamic equations can be derived systematically regardless of the coordinate system chosen. The derivation given below is based on the description of Lagrangian dynamics given in the text *Robot Analysis and Control* (Asada and Slotine 1986).

2.1.1 Lagrangian Formulation

If $q_1, \ldots, q_n$ are the generalized coordinates describing the orientation of a system, and T and U are the total kinetic energy and potential energy respectively, then the Lagrangian L is defined by

$$L(q_i, \dot{q}_i) = T - U \tag{2.1}$$

The equations of motion of the system are given by

$$\frac{d}{dt}\frac{\partial L}{\partial \dot{q}_i} - \frac{\partial L}{\partial q_i} = Q_i \qquad i = 1, \ldots, n \tag{2.2}$$

where Q_i represents the generalized force that corresponds with q_i, the joint angle coordinates.

Ultimately, the objective is to obtain a formula for calculating the inertia tensor of the system. First, however, the Jacobian matrices relating the geometry of the segments and their joint centers are expressed in the form

$$\begin{aligned} J_L^{(i)} &= \left[J_{L1}^{(i)} \ldots J_{Li}^{(i)} \;\; 0 \ldots 0 \right] \\ J_A^{(i)} &= \left[J_{A1}^{(i)} \ldots J_{Ai}^{(i)} \;\; 0 \ldots 0 \right] \end{aligned} \tag{2.3}$$

Each column vector is given by

$$J_{Lj}^{(i)} = \begin{cases} b_{j-1} & \text{for a prismatic joint} \\ b_{j-1} \times r_{0,ci} & \text{for a revolute joint} \end{cases}$$

$$J_{Aj}^{(i)} = \begin{cases} 0 & \text{for a prismatic joint} \\ b_{j-1} & \text{for a revolute joint} \end{cases} \tag{2.4}$$

where j represents the the column number in the Jacobian matrix, b_{j-1} is the 3 x 1 unit vector representing joint axis j-1, and $r_{0,ci}$ is the position vector to the centroid of segment i with reference to the base coordinate system. A prismatic joint allows only translational relative motion and a revolute joint only allows rotational relative motion between connected segments.

The total kinetic energy stored in the system is given by

$$T = \frac{1}{2}\sum_{i=1}^{n}\left(m_i \dot{q}^T J_L^{(i)T} J_L^{(i)} \dot{q} + \dot{q}^T J_A^{(i)T} I_i J_A^{(i)} \dot{q} \right) = \frac{1}{2}\dot{q}^T H \dot{q} \tag{2.5}$$

and is expressed in terms of the joint velocities $\dot{q} = \left[\dot{q}_1, \ldots, \dot{q}_n \right]^T$ that are the derivatives of the joint displacements $q = \left[q_1, \ldots, q_n \right]^T$ that represent a complete set of generalized

coordinates. The matrix H is known as the *manipulator inertia tensor*[1] and contains the mass properties of the complete arm linkage. This n x n matrix is obtained from the formula

$$H = \sum_{i=1}^{n} \left(m_i J_L^{(i)T} J_L^{(i)} + J_A^{(i)T} I_i J_A^{(i)} \right) \tag{2.6}$$

The manipulator inertia tensor is a symmetric positive definite matrix whose quadratic form relates to the kinetic energy. It is important to note that, since Jacobian matrices are involved, which vary with the orientation of the arm, the manipulator inertia tensor is configuration-dependent and represents the combined mass properties of the whole system for a given configuration. A consequence for computer simulations is that the terms of the matrix must be recalculated for each time interval during the execution of a movement, and this can significantly increase processing time.

The next step is to consider the generalized forces $Q = [Q_1, \ldots, Q_n]^T$ that account for all the forces and moments acting on the arm linkage other than the inertial and gravity forces. The generalized forces are identified as

$$Q = \tau + J^T F_{ext} \tag{2.7}$$

where τ represents the joint torques and F_{ext} represents the external forces acting on the system. Finally, the equations of motion are obtained from the expression

$$\sum_{j=1}^{n} H_{ij} \ddot{q}_j + \sum_{j=1}^{n} \sum_{k=1}^{n} h_{ijk} \dot{q}_j \dot{q}_k + G_i = Q_i \qquad i = 1, \ldots, n \tag{2.8}$$

where

$$h_{ijk} = \frac{\partial H_{ij}}{\partial q_k} - \frac{1}{2} \frac{\partial H_{jk}}{\partial q_i} \tag{2.9}$$

and

---

[1]Derived from robotic systems terminology.

$$G_i = \sum_{j=1}^{n} m_j g^T J_{Li}^{(j)} \tag{2.10}$$

Note that H_{ij} represents the term or expression in the i-th row and j-th column of H. The first term in equation 2.8 accounts for the inertial torques, the second term represents the centrifugal and Coriolis effects, and the third term is the torque due to gravity. This formulation directly provides the closed-form dynamics equations.

2.1.2 Equations of Motion for a Two Degree of Freedom Arm

When the general Lagrangian equations given above are applied to the specific case of the two segment, two degree of freedom arm illustrated in Figure 2.1, the following equations of motion are obtained:

$$\begin{aligned} H_{11}\ddot{q}_1 + H_{12}\ddot{q}_2 + h_{122}\dot{q}_2^{\,2} + (h_{112} + h_{121})\dot{q}_1\dot{q}_2 &= \tau_1 \\ H_{22}\ddot{q}_2 + H_{12}\ddot{q}_1 + h_{211}\dot{q}_1^{\,2} &= \tau_2 \end{aligned} \tag{2.11}$$

The manipulator inertia tensor is given by

$$\mathbf{H} = \begin{bmatrix} m_1 l_{c1}^2 + I_1 + m_2(l_1^2 + l_{c2}^2 + 2l_1 l_{c2}\cos q_2) + I_2 & m_2 l_1 l_{c2}\cos q_2 + m_2 l_{c2}^2 + I_2 \\ m_2 l_1 l_{c2}\cos q_2 + m_2 l_{c2}^2 + I_2 & m_2 l_{c2}^2 + I_2 \end{bmatrix} \tag{2.12}$$

where

$$\begin{aligned} &h_{122} = -h \;,\; h_{112} + h_{121} = -2h \;,\; h_{211} = h \;, \\ &\text{and} \quad h = m_2 l_1 l_{c2}\sin q_2 \end{aligned} \tag{2.13}$$

The lengths l_{c1} and l_{c2} are measure from the joint center to the corresponding segment's center of mass. Note that the gravity terms normally appearing in the equations of motion have dropped out due to the weightless environment. Also, only joint torques appear on the right hand side of the equations of motion (2.11) since it has been assumed that there are no external forces acting on the arm.

Fairly complex equations of motion are seen for a relatively simple dynamic system. As more segments and more degrees of freedom are added, not only do the individual elements of the manipulator inertia tensor become longer expressions, but also the number of elements increases according to the square of the number of degrees of freedom. Clearly, it soon becomes impractical to formulate the equations of motion by

hand. It is for this reason that so much effort has been invested in developing computer programs that formulate the equations computationally. The simulation methods and results presented in the remainder of this report take advantage of, and build upon, powerful computational techniques that have been developed for the purpose of analyzing more complicated dynamic systems.

2.2 STS-63 Spartan Mass Handling EVA Task

Before delving into the details of how the simulations are performed, it is helpful to consider a brief description of the actual EVA on which the simulations were modeled. The Spartan spacewalk, performed on Space Shuttle mission STS-63 in March 1995, had two primary objectives: firstly, to test the use of thermal insulation in the EMU gloves in cold attitude operations (crewmembers in shadow) and to gain experience with handling large masses. It is the second objective that serves as the subject task for simulation.

A free flying payload, the Spartan 204 astronomy spacecraft, served as the mass handling test object for the EVA crewmembers. A NASA photograph image of the astronauts with Spartan is shown in Figure 2.2. Although the Spartan 204 was designed to be deployed and berthed by means of the Orbiter's Remote Manipulator System (RMS), or robot arm, a contingency EVA was planned in which manual berthing of the payload could be achieved in case of a failure of the nominal RMS berthing procedure. Contingency EVAs are often planned, and trained for, with free flying payloads of this type, although, other than the opportunities presented during the Hubble space telescope repair mission, little experience has been gained in the manipulation of objects with significant inertial properties.

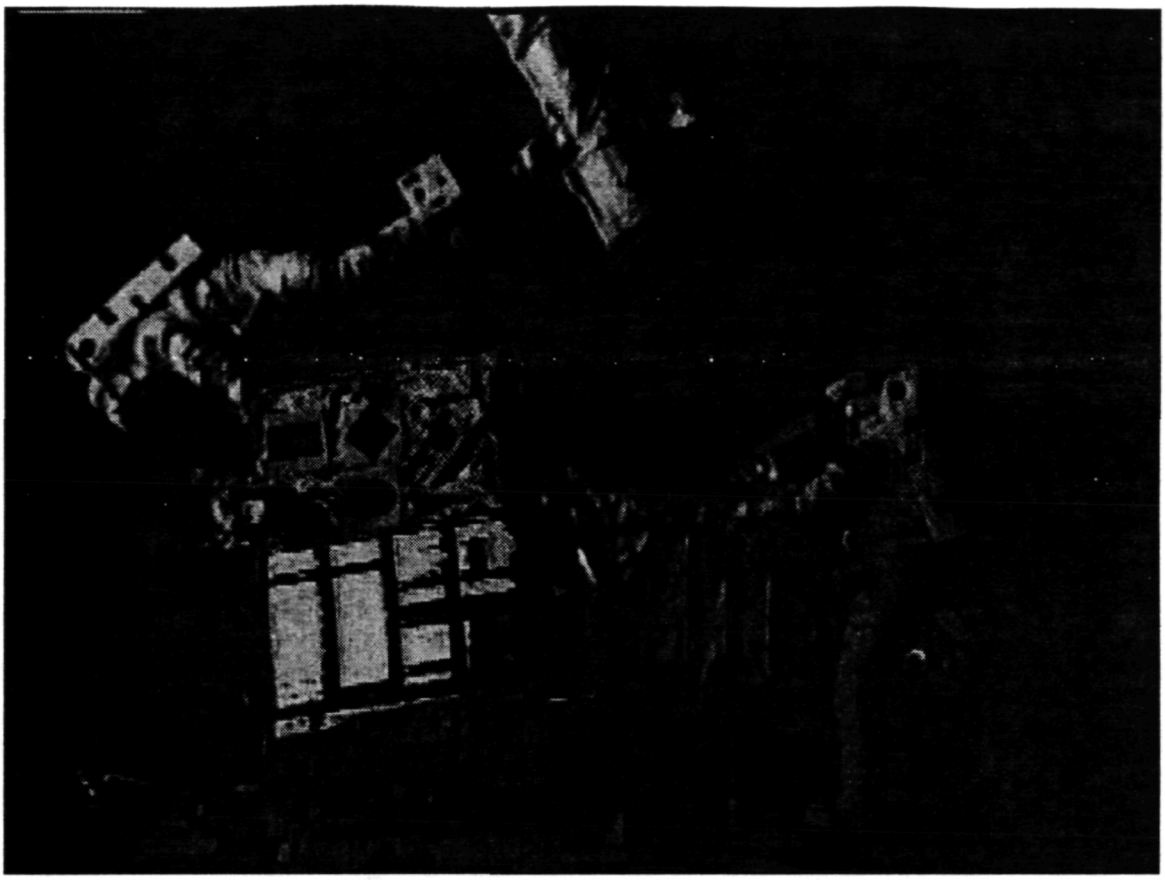

Figure 2.2 EVA crewmembers with Spartan 204 free flyer payload. (Source: NASA)

ORIGINAL PAGE IS
OF POOR QUALITY

In addition to the contingency procedure, it was proposed that Spartan could be used for a scheduled EVA in which crewmembers could practice handling this massive object as a way of preparing for similar mass manipulation tasks to be performed very often during the construction and servicing of the international space station. The mass properties for the Spartan free flyer are presented in Table 2.1.

Table 2.1 Mass property data for Spartan 204 free flyer

Mass: 1,201.07 kg (82.30 slugs)	**Moments of Inertia:**
	I_{xx} = 325.73 kg-m^2 (240.31 slug-ft^2)
Center of Mass (PAS†):	I_{yy} = 352.28 kg-m^2 (259.90 slug-ft^2)
X = 0.622 m (2.04 ft)	I_{zz} = 334.79 kg-m^2 (246.997 slug-ft^2)
Y = -0.481 m (-1.58 ft)	
Z = 0.572 m (1.88 ft)	**Products of Inertia:**
	I_{xy} = -3.75 kg-m^2 (-2.77 slug-ft^2)
	I_{xz} = 92.67 kg-m^2 (68.37 slug-ft^2)
	I_{yz} = -28.34 kg-m^2 (-20.91 slug-ft^2)

† PAS = Payload Axis System, defined with respect to the bottom left corner on the thermal louver side.

The most striking value in Table 2.1 is the Spartan payload's mass, which is more than fifteen times the mass of an average crewmember (not including EMU). Clearly, this represents a far greater mass than anything a person might have experience handling in a one-g environment.

While it is true that in a weightless condition one can theoretically move objects of unlimited size, any relative kinetic energy that the crewmember imparts to the object must similarly be removed by the crewmember if he wishes to keep hold of it. The crewmember could find himself trapped between two objects (i.e., the payload and the RMS or Orbiter), or forced into limb hyperextension, resulting in bodily injury or damage to the spacesuit, if he does not anticipate the object's motion.

It is difficult for astronauts and mission operations personnel to predict, at any quantitative level, the types of loads that might be experienced in handling large objects in weightlessness, both because of the lack of empirical data on this procedure and lack of analytical models of the multibody dynamics involved. The prime objective of this study is to demonstrate how a computer program, which combines the mathematical rigor of computational multibody dynamics and the communicative strengths of animation and

data plots, might be used to predict the quantitative and qualitative aspects of human performance in extravehicular activity. The sections below describe how this objective was pursued.

2.3 Simulation Objectives

The particular scenario that is modeled during these simulations is that of an EVA crewmember manipulating the Spartan 204 free flyer along a particular trajectory at constant speed. A circular trajectory of radius 0.15 m with an angular velocity of 0.628 radians per second (one complete revolution in ten seconds) is prescribed for the center of mass of the crewperson's hand. The orientation of the Spartan payload remains fixed with no angular velocity being imparted. Translations are confined to the vertical plane. It is assumed that the astronaut maintains a rigid grip on a handle attached to Spartan.

It is necessary, at this point, to distinguish between the terms *endpoint coordinates* and *joint coordinates*. The relationship between the two systems is illustrated in Figure 2.3. Endpoint coordinates refers to the description of the position and orientation of the end-effector of a multibody chain dynamic system (typically a robot arm or a human limb). Usually, an endpoint coordinate system is specified at a particular point on the last body in the chain. The position and orientation of the coordinate system is described in reference to the global coordinate system, usually fixed in an inertial reference frame. Joint coordinates, on the other hand, describe the state of the multibody system in terms of the angular orientations (or linear displacements in the case of sliding joints) of the bodies, with respect to either the inboard body or the global coordinate system (called "generalized" coordinates). The two coordinate systems are related through the Jacobian matrix of the system.

There is an important difference between the two coordinate systems. While the joint coordinate system always describes the state (configuration) of a system uniquely, a description of the state of a system in terms of endpoint coordinates may not specify the system's configuration uniquely if there are redundant degrees of freedom. A redundant degree of freedom condition arises when there are more joint coordinates than endpoint coordinates. The problem introduced for inverse kinematics is that there may be multiple configurations (or states) of a system producing a given endpoint state. At the same time, in terms of inverse dynamics, this means that there may be different joint torque (and force) solutions that satisfy the given end-effector forces and torques. The geometric ambiguity is shown by means of the dashed outline in Figure 2.3 (Configuration 2).

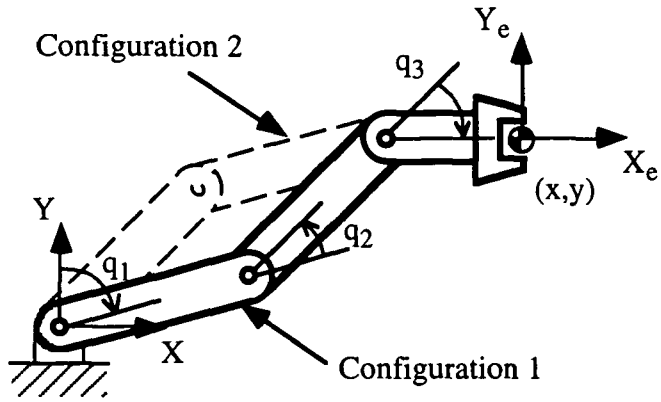

Figure 2.3 Illustration of joint coordinates and endpoint coordinates and occurrence of multiple solutions in systems with redundant degrees of freedom.

It is particularly desirable to be able to specify the motion to be performed by the crewmember in terms of endpoint coordinates only, that is in terms of the X and Y positions of the c.m. (center of mass) of the hand. Describing the motion in this manner demonstrates that it is possible to perform a simulation by knowing only the motion data associated with the task itself, without the need to explicitly prescribe the motion being performed in terms of joint coordinates. Only the initial angles for the wrist, elbow, shoulder, hip, knee, and ankle joints need be known. The subsequent time histories of position, velocity, acceleration, and torque for these joints are calculated during the simulation. The importance of this capability is that it allows analysts, astronaut trainers, or mission operations personnel, to describe the parameters of an EVA task to be simulated in a simple pragmatic way and does not require them to do extensive analysis beforehand.

Thus the objectives of the dynamic simulation may be summarized as follows:

1) Determine the kinematics (in joint coordinates) of the crewmember's motions given only a description of the manipulation task (in endpoint coordinates).

2) Perform an inverse dynamics computation to determine the joint torques in the ankle, knee, hip, shoulder, elbow, and wrist.

3) Compare the calculated values with empirical human physiological limit data such as joint angle limits and maximum torque availability based on joint position and velocity.

4) Demonstrate how accuracy and realism can be improved in successive simulations.

2.4 Dynamic Simulation

The purpose of this section is to describe in greater detail how the simulation is actually carried out on the computer. Various phases may be identified: the creation of a system description file; formulation of the equations of motion using SD/FAST; development of simulation code, including steps to perform a validation of the model based on test values of joint torque, followed by inverse kinematics and inverse dynamics; comparison with physiological limits; and animation with data plots.

2.4.1 System Description

The first step in the development of a simulation is to develop a model of the multibody dynamic system under consideration. It is highly advisable to design the simplest possible model which is capable of satisfying the objectives of the simulation. Starting with a simple model facilitates the steps of error elimination and model validation in the early stage of a simulation. Once the rudimentary system model is operating correctly, one can expand the complexity of the model incrementally while verifying the validity of the model each time it is changed. Due to the inherent complexity of multibody dynamics, this turns out to be a very wise philosophy in practice.

In considering the structure of the human body, one might be inclined to think that the simplest model should include fourteen segments: two feet, two lower legs, two upper legs, a torso, a head, two upper arms, two forearms, and two hands. Certainly, models of much greater complexity can be imagined. For example, if the full articulation of the hands are to be modeled, then 19 degrees of freedom must be incorporated for each hand. However, it is also possible to use simpler models of the human body depending on the degree of localization of motion and the amount of detail required. For instance, if a task is accomplished almost exclusively by means of arm motions, then one might be able to assume that the torso is fixed in inertial space (thus becoming the "ground" segment) and model the arm simply as a three segment system. In addition, symmetry can often be exploited in both the model and the simulation. If a manipulation task is carried out in

which both arms perform the identical motion, then it may be possible to model both arms as a single arm, that is modeling the six segments as only three, but with double the mass properties of each segment. Once the torques have been determined, they may be divided in half to yield the contribution of each separate arm. This strategy relies on the assumption that mass properties and torques may be combined in a linear fashion when they occur in parallel.

Since the task being analyzed involves the manipulation of an object along a trajectory confined to the median plane of the crewmember, the limbs on the left and right sides of the body perform identical motions. In addition, it is assumed that the feet of the astronaut are rigidly fixed to a body of large inertia and thus can be considered to be part of the "ground" segment and not part of the dynamic system under consideration (A foot restraint would serve this purpose in practice; although a more advanced model might consider the compliance of the foot restraint, the RMS, and perhaps the Orbiter too.). Given these simplifications, it is possible to model the astronaut's body by means of seven segments with the Spartan 204 spacecraft as an eighth segment "welded" to the hand. A sketch of this system is shown in Figure 2.4. The segments are: lower leg, upper leg, torso, head, upper arm, forearm, hand, and Spartan.

To make it possible to specify the motion in terms of endpoint coordinates, the model makes use of an interesting trick. The explanation of this is aided by Figure 2.4. Up to this point, the crewmember's body is represented by a tree structure (no loop joints). In fact the articulated bodies, from the lower leg connected to ground, to the hand as the outermost body, represent a simple chain-link structure. The hand, however, is defined with half the density, and thus half the mass properties, of the intended hand for reasons that are explained below. An additional tree is now defined. Starting at ground (ankle joint), a massless body is created with an offset equal to the distance between the ankle and the center of mass of the hand and "attached" to ground by means of a slider in the X-direction. Another massless body is defined and attached to the first massless body by means of a slider in the Y-direction. This massless body is then pinned (axis in the Z-direction) to another body with half the mass and moments of inertia of the intended hand. This half-hand is welded to the half-hand attached to the fore-arm, thus completing a loop structure. The resulting hand has the mass and moments of inertia of a full hand. In this way it is possible to manipulate the arm and body of the crewmember in the X-Y plane by prescribing the motion of the center of mass of the hand in global Cartesian coordinates in terms of the sliding displacements of the two massless bodies.

The next step is to create a system description file. It is advisable to store this file in a separate directory bearing the name of the simulation. This directory will then also

contain the files generated by SD/FAST, the simulation code, and the output data files. The filename itself will be of the form <file>.sd, where <file> is chosen to be representative of the simulation and serves as the root for other files generated by SD/FAST. The system description file is simply a means of conveying to SD/FAST the relevant parameters and geometry of the system so that the equations of motion can be formulated. Full details on how this input file should be created can be found in the SD/FAST user's manual (Hollars, Rosenthal et al. 1994). The system description file for the eight segment model used in this simulation is presented in its entirety in Appendix A. A summary of the basic elements of this file will be presented here with examples taken from the actual system description file used in the simulation.

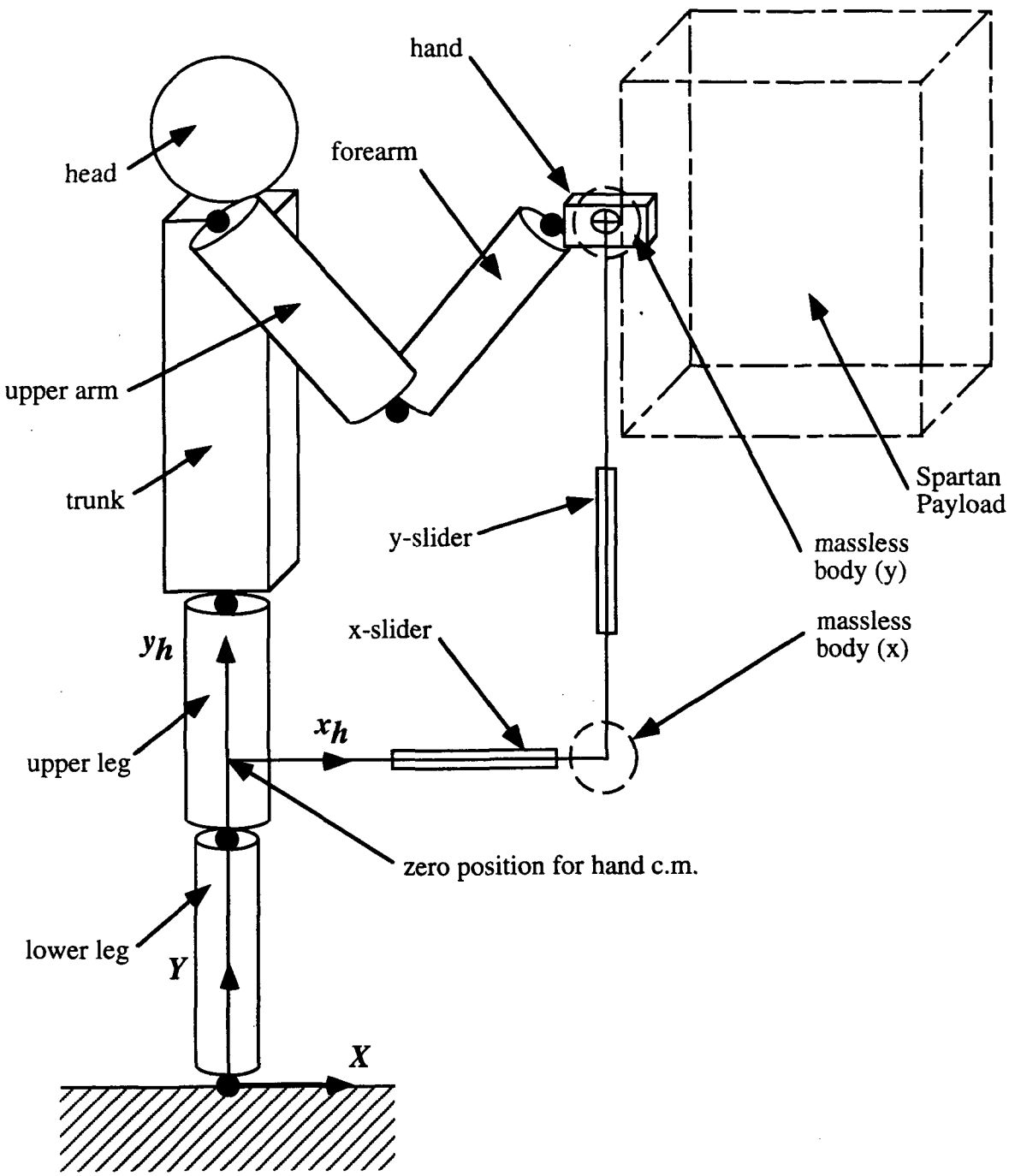

Figure 2.4 Sketch of eight segment system showing massless bodies and sliding joints for prescribing motion of center of mass of hand.

The first part of the system description file consists of comment lines which normally indicate the name of the file, the author, date of last revision, and a short description of the nature of the system. Other comment lines are added at appropriate points in the body of the file. The second part is normally a "preamble" which includes any keywords relevant to the entire system. An example of this would be the specification of gravity, e.g., "gravity = 0 -9.8 0", but in this case gravity has been zeroed out since the situation being simulated is assumed to occur in weightlessness. The third major part of the file consists of one or more "body paragraphs". Each of these specifies the relevant parameters of a body and how it is connected to other bodies in the system. All vectors and mass properties for the bodies are specified according to a reference configuration. It is advisable to choose a reference configuration that makes it as simple as possible to describe the vectors and mass properties. Wherever possible, the principal axes of each body should be aligned with one or more axes of the global coordinate system. The reference configuration for this simulation is shown in Figure 2.5. An example body paragraph is given below:

```
body = uleg                 inb = lleg      joint = pin     prescribed = ?
mass = 17.300               inertia = .294244 .055360 .294244
bodytojoint = 0 -.215 0     inbtojoint = 0 .215 0   pin = 0 0 1
```

The first keyword "body" is followed by the name of the body, "uleg" for upper-leg in this case. Next the keyword "inb" identifies the inboard body in the structure, which in this case is "lleg" for lower-leg. One of the bodies in the system must be connected to ground in some way and this is accomplished by assigning "$ground" to "inb". Next comes the joint specification. In the example above, this is simply a one d.o.f pin joint. The specification "prescribed = ?" notifies SD/FAST that prescribed motion may be used as an option for articulating this body. The question mark makes it possible to turn prescribed motion on and off from within the simulation driver code. The second line in this example specifies the mass and inertial properties of the body in SI units. If only three values follow the keyword "inertia" then it is assumed that these are the principal moments of inertia. It is possible, however, to specify a full 3 x 3 inertia tensor for an asymmetrical body. The last line contains three vectors describing the geometric state of the body when the system is in its initial reference configuration. (The reference configuration for this system, shown in Figure 2.5, has the astronaut standing up straight with his arms hanging straight down next to his sides.)

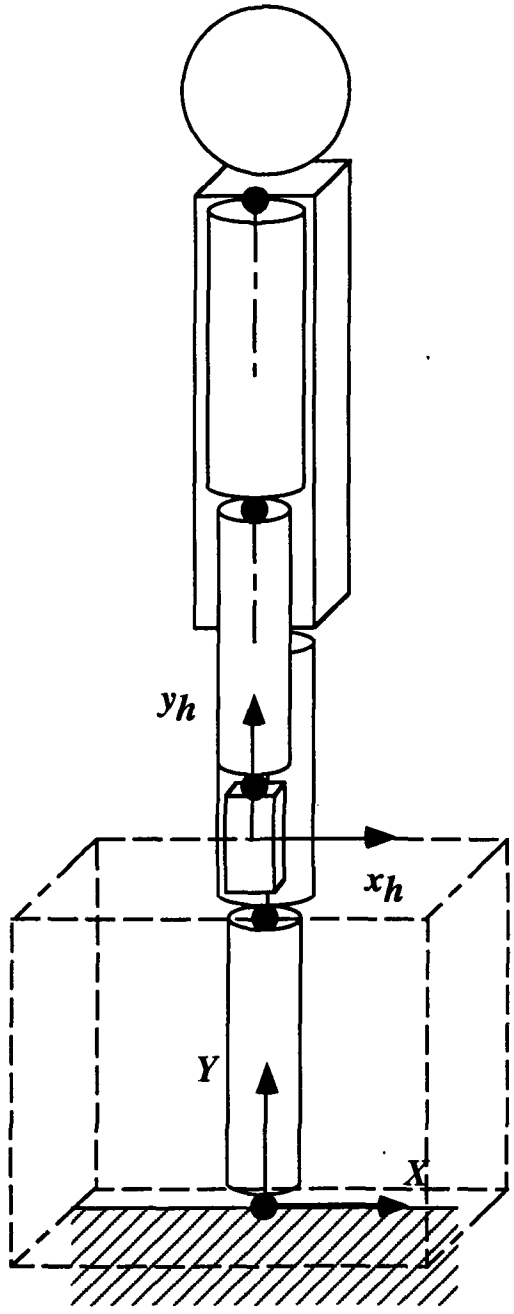

Figure 2.5 Reference configuration for description of dynamic system.

The first vector, "bodytojoint", extends from the body's center of mass to the joint connecting it to the inboard body. The second vector "inbtojoint" extends from the center of mass of the inboard body to the same joint. The last vector describes the direction of the joint axis (the axis of rotation, in the case of a pin or revolute joint, or the axis of translation for a sliding joint). Only the direction of this vector matters, so it is common to present it in a normalized form. Several of these body paragraphs make up the bulk of the system description file. Most of them follow the same format described above, however, one of these paragraphs is slightly different. This paragraph is

```
body = hslide      inb = harm     joint = weld
    bodytojoint = 0 0 0    inbtojoint = 0 0 0
    pin = 0 0 1            bodypin = 0 0 1
    inbref = 0 1 0         bodyref = 0 1 0
```

The code given above does not represent an actual body, but is used to tell SD/FAST how to weld the two halves of the hand together. The vectors "pin", which must align with "bodypin", and "inbref", which must align with "bodyref" and is perpendicular to the "pin" vector, are used to ensure that the two parts are welded together in the appropriate relative orientation. Since the weld joint connects two tree structures together, that originate from the same base (ground), it constitutes a "loop" joint.

2.4.2 Formulation of Equations of Motion

Once the dynamic system has been fully specified in the system description file, the next step is to process the system description file using SD/FAST. This step is a fairly easy one for the analyst. SD/FAST is invoked by simply typing

```
sdfast -lc
```

at the UNIX shell prompt. The "-lc" option tells SD/FAST to generate code in the C language. The name of the system description file can either be specified in the command line or entered when prompted by SD/FAST. If no syntactical errors are found and the input file is successfully processed, several new files are created: a Dynamics File (identified by <file>_dyn.c) that contains subroutines (or "functions" for C code) specific to the dynamic system and representing the equations of motion numerically; an Information File (identified by <file>_info) containing text and various parameters of use in creating the simulation driver code; and an Analysis File (identified by <file>_sar.c)

containing simple analysis routines that can be called during simulation runs. When the simulation driver code has been written, it is compiled and linked along with the Dynamics File and the Analysis File. Once again, a more detailed description of this step can be found in the SD/FAST user's manual. The next three sections describe the three major parts of the simulation driver code which is presented in its entirety in Appendix B.

2.4.3 Joint Torque Test Functions

The first step in the simulation is to verify the validity and accuracy of the dynamic model by executing three test functions which return torque values for the shoulder, elbow, and wrist. Only the arm joints are tested since it is the arm motions and torque values that are of primary interest in this simulation. By choosing a trivial configuration and simple motion, it is possible to calculate torque values for each of the joints by hand and these are compared with the values returned by the computer simulation.

The initial configuration of the body is with the lower leg, upper leg, and trunk straight up, as in the reference configuration, but with the arm straight out in a horizontal position. This configuration is shown in Figure 2.6.

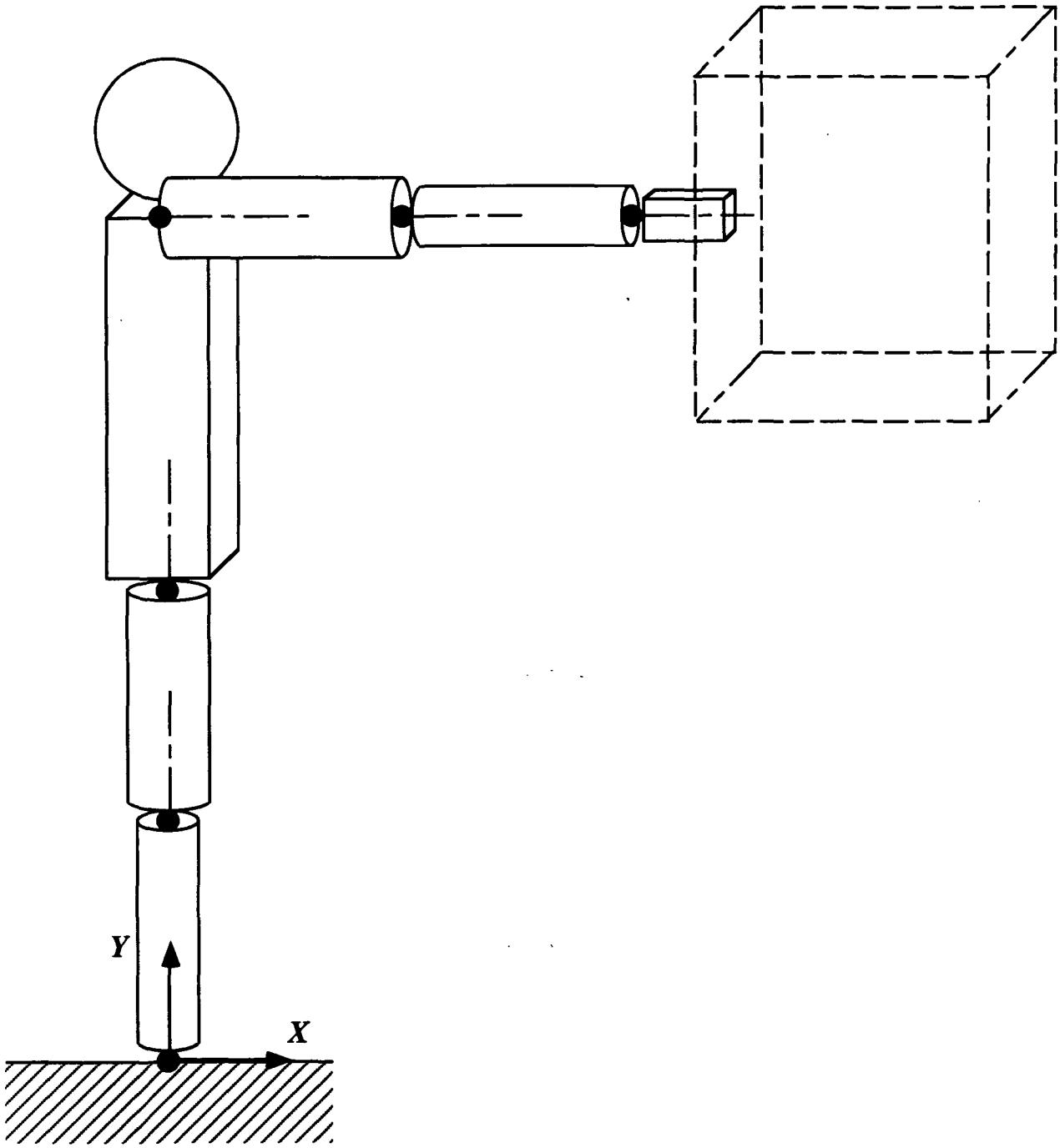

Figure 2.6 Initial configuration of system for application of test functions.

During each of the three phases, one of the joints is assigned a prescribed acceleration of 5 deg/sec^2 while all the other joints (including the hip, knee, and ankle) are assigned a prescribed acceleration of 0 deg/sec^2. In this way the bodies outboard of the test joint rotate as if they were one rigid body, while the bodies inboard of the test joint remain fixed because they are ultimately joined to ground at the ankle joint. For the outboard bodies moving in unison, it was possible to calculate their combined mass moment of inertia using the parallel axis theorem

$$I = \sum_{i=1}^{n} (I_{c.m.} + d^2 m)_{(i)} \tag{2.14}$$

where

I = total moment of inertia
$I_{c.m.}$ = moment of inertia of body i with respect to its center of mass
d = distance of body i center of mass from the joint under consideration
m = mass of body i
n = number of bodies outboard of joint under consideration

The torque applied at a joint can be calculated from the effective moment of inertia of the outboard bodies and the acceleration at the joint using the rotational (Euler) form of Newton's second law, $\tau = I\alpha$. A comparison of the computer calculated and hand calculated torque values for these test functions is presented in the next chapter.

2.4.4 Inverse Kinematics

The next step in the simulation is the inverse kinematics phase. It is termed *inverse* kinematics because only the motion of the endpoint is prescribed and this is used to determine the corresponding motion of the system in terms of joint coordinates. Before executing the motion, it is necessary to place the system in its initial configuration. It was chosen to place the trunk and legs in the neutral body posture for weightlesssness as specified in NASA Man Systems Standard 3000. The joint angles for an unsuited crewmember are used since no values for neutral body posture for a spacesuited crewmember could be found. The arms are placed in an initial configuration that allows for the Spartan 204 to be conveniently manipulated along a circular trajectory.

To simplify the simulation, it was specified that the ankle, knee, and hip joints should remain fixed at their starting angles. This was accomplished by prescribing zero angular acceleration and zero velocity for each of these joints. In addition, the hand is maintained

in a fixed orientation so that the Spartan payload does not rotate as the hand follows the prescribed trajectory. By simplifying the motion in this way, the redundant degrees of freedom are canceled by the constraints and only two remaining degrees of freedom, in the elbow joint and shoulder joint, remain to match the two degrees of freedom in the endpoint (hand) coordinates. This strategy is in keeping with the philosophy of getting a simpler simulation to work before modifying it to represent a more complex situation.

The simulation system is able to obtain solutions to inverse kinematics when redundant degrees of freedom are present by employing a linearized least squares root finder to determine the joint angles (and their derivatives) required to achieve the prescribed endpoint motion. If more degrees of freedom are allowed, however, then it becomes necessary to implement some form of control in some of the joints or unrealistic motion will result. More explicitly, if all the joints in the body are passive, and the hand is "dragged" along a certain trajectory, then the body will behave somewhat like a rag-doll where its posture is determined only by the mass properties of the segments. One way of controlling the posture of the body is to specify springs and dampers at certain joints which apply torques in proportion to the displacement and angular velocity of those joints. These springs and dampers mimic the passive behavior of muscle groups actuating a joint in the human body. The simulation can be modified slightly by including torsional springs and dampers in the ankle, knee, and hip joints. These joints then seek to achieve a certain prescribed angle but are allowed some play based on the compliance of the springs and dampers and this results in a somewhat more realistic motion than the rigid posture obtained by fixing the joint angles. This technique is implemented in a second simulation.

The inverse kinematic phase of the simulation now proceeds with the lower leg, upper leg, and trunk segments maintaining a fixed position while the upper arm, forearm, and hand move in appropriate ways to follow the circular trajectory while satisfying the constraints mentioned above. A circle was chosen as the trajectory because of its simplicity and because the smoothness reduced the peak accelerations (and thus peak forces and moments) required in the arm joints. To follow a square path at a constant speed, for instance, would require infinite accelerations (and infinite loads) in the joints at the corners. The initial configuration of the body and the circular trajectory followed by the hand are shown in Figure 2.7.

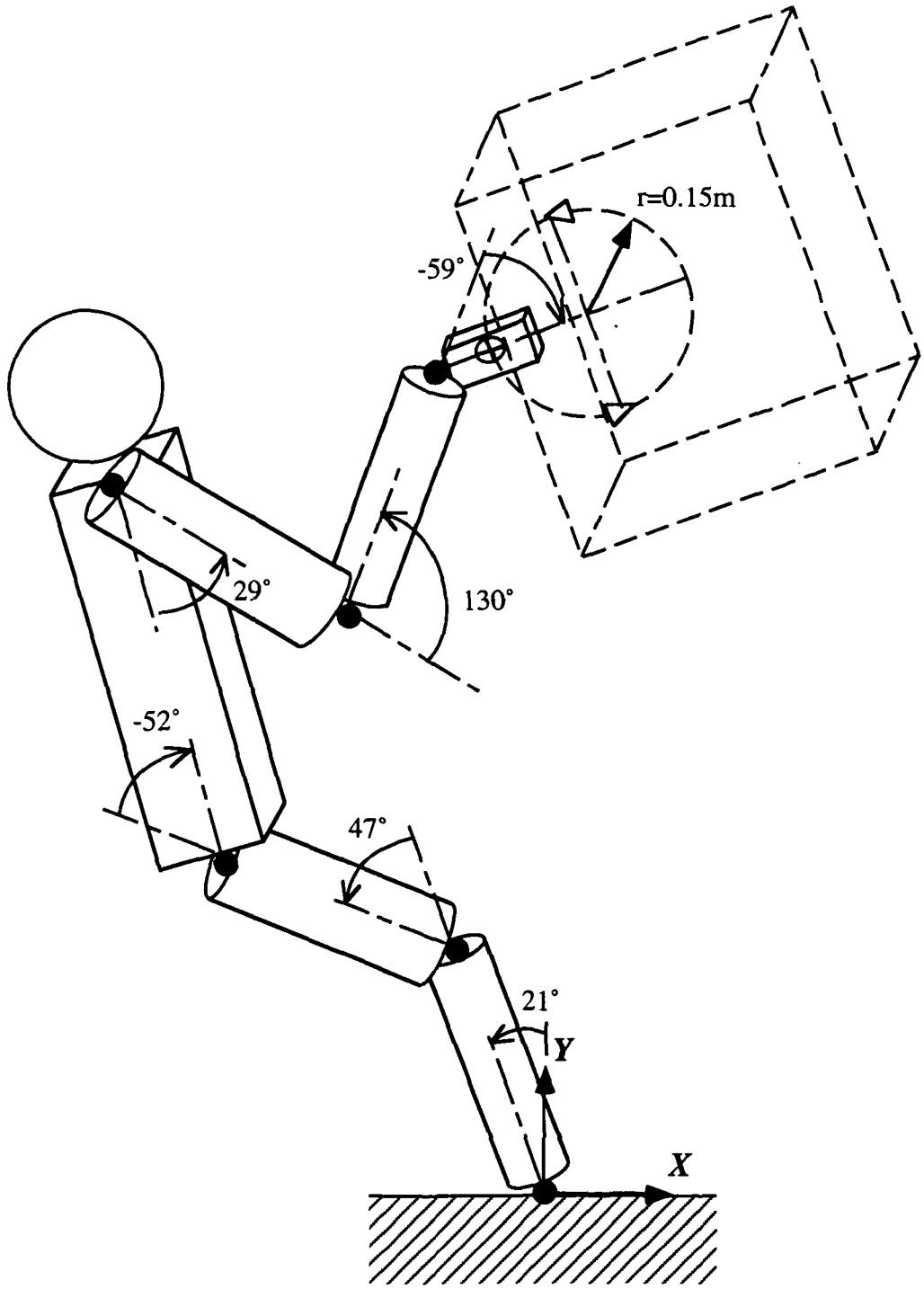

Figure 2.7 Initial configuration for first simulation and prescribed circular trajectory of hand.

The initial conditions are obtained by performing an assembly and initial velocity analysis through calls to SD/FAST routines. The outcome of these calls is a fully compatible state vector (the first half of the state vector represents all the position values in the system, and the second half represents all the velocity values.) Following this, the simulation code calls a routine which integrates the arm motion repetitively through small time steps (0.05 sec was used) until the full trajectory is completed. During each time step, the position, velocity and acceleration of the center of mass of the hand were prescribed using the following expressions:

$$\begin{aligned}
&\theta = \pi + \omega t \\
&\begin{cases} x_{cm} = x_{start} + r(1+\cos\theta) \\ y_{cm} = y_{start} + r\sin\theta \end{cases} \\
&\begin{cases} \dot{x}_{cm} = -\omega r\sin\theta \\ \dot{y}_{cm} = \omega r\cos\theta \end{cases} \\
&\begin{cases} \ddot{x}_{cm} = -\omega^2 r\cos\theta \\ \ddot{y}_{cm} = -\omega^2 r\sin\theta \end{cases}
\end{aligned} \tag{2.15}$$

where,

ω = angular velocity
r = radius of circular trajectory

At each incremental time step during the motion simulation, the values for position, velocity, and acceleration of each joint in the body (excluding the sliding joints connecting the massless bodies) are recorded in a two dimensional state-time array. These values are subsequently recalled in a "playback" mode during the inverse dynamics phase described next.

2.4.5 Inverse Dynamics

During the inverse dynamics phase of the simulation, the values of joint position, velocity, and acceleration determined during the inverse dynamics phase are recalled and used to prescribe the motion of the system in a "playback" mode. Prescribed motion is turned "on" for the pin joints and "off" for the sliding joints and the one pin joint connecting a massless body to the hand. After each time step, the joints are assigned the prescribed values associated with the point in time during the motion and the simulation calls an SD/FAST function, called "sdhinget", for each joint to determine what torque is

required in that joint to achieve the required motion. The resulting time histories for torque are presented in the next chapter.

2.5 Comparison with Physiological Limits

Once the data for the position, velocity, acceleration, and torque of the joints has been obtained, it can be further analyzed to evaluate the physiological state of the crewmember in the simulation. It is of interest to compare the values obtained with human physiological limits such as joint range of motion and muscle strength.

Due to the preliminary nature of this simulation and the philosophy of beginning with a simple case, there is as yet no mechanism built into the simulation which enforces the physiological limits of human motion. The joint position, velocity, acceleration, and torque values calculated are entirely theoretical and represent the values required to accomplish the manipulation task while obeying the laws of multibody dynamics. There is no guarantee that these values fall within the range of human capability. For this reason, it is very useful to compare these theoretical values with experimentally determined values of human performance. Of particular interest are the limits of joint range of motion and of maximum joint actuation strength. Joint range of motion limits are obtained from the "NASA Man-Systems Integration Standards" (NASA 1987) and are plotted along with the theoretical values of joint angle. Joint actuation strength is represented by torque values as a function of joint angle and joint velocity. These maximum torque values are obtained from a human strength model developed by the Anthropometrics and Biomechanics Laboratory at NASA's Johnson Space Center (Pandya, Hasson et al. 1992; Pandya, Maida et al. 1992).

2.6 Animation and Data Display

An animation and data display program called EVADS (EVA Dynamic Simulation) has been developed for the purpose of communicating graphically both qualitative and quantitative information about the simulation. Both animation and data plots are displayed simultaneously so that the plots can be correlated with the three dimensional image of the system.

Data for this program is input in the form of text files created by the simulation driver code. Due to the large quantity of data, especially in systems that have several segments, four separate files are input for position, velocity, acceleration, and torque data. In the future it is hoped that this program can be linked with the simulation driver code so that the simulations can be controlled in a more visually interactive manner.

The three-dimensional rendered images in the animation are of great help to the analyst. One can determine at a glance whether the overall system starts off with the correct initial configuration and executes motion that makes sense. The user can very conveniently alter the viewing angle and size of the animation image by means of the mouse controls and simple keystrokes.

The data is plotted below the animation portion of the window. At present, only one data category (e.g., elbow torque) can be plotted at a time, but there are plans to allow multiple plots to be displayed simultaneously in the future. The parameter to be displayed is selected from an array of virtual buttons arranged vertically along the right side of the screen. The plot itself is displayed in green with a fine grid in the background. The vertical axis displays the parameter chosen and the scale is automatically chosen to accommodate the limiting values in the data set. The horizontal axis always displays time and the scale is fixed. To allow for time histories of varying length, however, the horizontal axis has the ability to scroll left and right. The point in time representing the state of the animated image is identified on the plot by means of a red vertical line. During the course of an animation run, this line moves along the plot in synchronization with the animated image. It is also possible to step through the animation manually, either forwards or backwards, using the ">" and "<" keys respectively. This mode is particularly useful for observing various parameters at specific points in time during the simulation and for debugging. Figures showing the computer images generated by EVADS are presented in the next chapter.

3. Results

This chapter presents the results of two dynamic simulations. The multibody model and associated system description file is the same for both simulations. Equations of motion are formulated by SD/FAST (using Kane's method) and represented in an implicit computational form. Specific simulation code performs four analyses on the dynamic system: joint torque test functions, assembly and initial velocity analysis, inverse kinematics, and inverse dynamics. The data is then visualized on the computer by means of three dimensional rendered animation and parameter time history plots.

The following sections present the results of: a comparison between the computer calculated and hand calculated joint torques for the test functions; the numerical results of the first simulation; the numerical results of the second simulation; and the animation and parameter plots of the EVADS interface. Numerical results for each of the two simulations are described in two subsections: data obtained from the inverse kinematics phase (joint angles, velocities, and accelerations) and joint torques obtained from the inverse dynamics phase.

3.1 Joint Torque Test Functions

The correlation between the hand calculated and computer calculated torque values for the test conditions described in the previous chapter are shown in Table 3.1. Considering that the parallel axis theorem was used to approximate the moments of inertia of segments moving in unison, the correspondence between values is remarkably good. The percent error was calculated by subtracting the torque values from the computer simulation from the hand calculated torque value, dividing the difference by the former, and multiplying by 100. The largest error, a value of -0.030 %, occurs in the wrist joint. While this value is still very low, the slightly larger error is probably accounted for by the close proximity of the wrist joint to the center of mass of the Spartan payload, reducing the accuracy of the parallel axis approximation.

Table 3.1 Comparison of hand calculated and computer simulation torques for test conditions in shoulder, elbow, and wrist joint.

Joint	Torque from Hand Calculation [N-m]	Torque from Computer Simulation [N-m]	Percent Error
Shoulder	211.441	211.419	+0.010
Elbow	138.196	138.210	-0.010
Wrist	86.951	86.977	-0.030

3.2 Simulation No. 1 - Fixed Lower Body

Two simulations of an EVA task were run. In the first simulation, the lower body joints (ankle, knee, and hip) were held in fixed positions, while in the second simulation, the lower body joints were given some compliance by means of virtual springs and dampers representing the passive mechanical properties of these joints. The numerical results of each simulation run are presented in a series of four figures. The first three categories, namely, joint angle, joint velocity, and joint acceleration are presented in this subsection for the fixed lower body simulation. Joint torques are presented in the following subsection. Each of the figures consists of a composite of six subplots depicting the data obtained for the ankle, knee, hip, shoulder, elbow, and wrist joints. In each case the relevant parameter is plotted against time as the independent variable. In all cases the curve depicting the actual kinematic or dynamic state of the system is shown as a solid line. Where limits on the parameter are available, for instance joint range of motion or maximum torque, the upper limit is plotted as a dashed line while the lower limit is plotted as a dash-dot line. For convenience, this key is summarized in Table 3.2 below. In viewing the plots it should be noticed that the vertical axis varies according to the range of data values represented. The automatic scaling of the plots helps to bring out details, but should be carefully considered when comparing plots with one another. The complete set of numerical data used to create the plots of the various system parameters and their limits is available in a separate document held at the MIT Man-Vehicle Laboratory. For conciseness, this chapter lists values only for specific conditions, such as the maxima and minima of each relevant parameter.

Table 3.2 Key for interpreting multi-curve plots.

Curve	Line Type
Upper Limit	--------
Actual State of System	_____
Lower Limit	-.-.-.-.-.

Before looking at the numerical data in depth, it is helpful to obtain a mental picture of the simulation run. For this reason, a composite of six images is shown in Figure 3.1. Each of these images shows the state of the system at intervals of 2.0 seconds, beginning with the initial configuration and ending with the final configuration. In this case, the initial and final configurations are exactly the same since the motion involves manipulating the object through a circular trajectory.

It can clearly be seen how the lower body (lower leg, upper leg, and trunk) is stationary, while the motion is carried out by the arm segments alone. Notice also that the Spartan payload is kept at a constant orientation throughout the simulation and experiences only translational motions. The next subsection presents the results of the inverse kinematics analysis in the first simulation, followed by a subsection presenting the joint torques found in the inverse dynamics analysis.

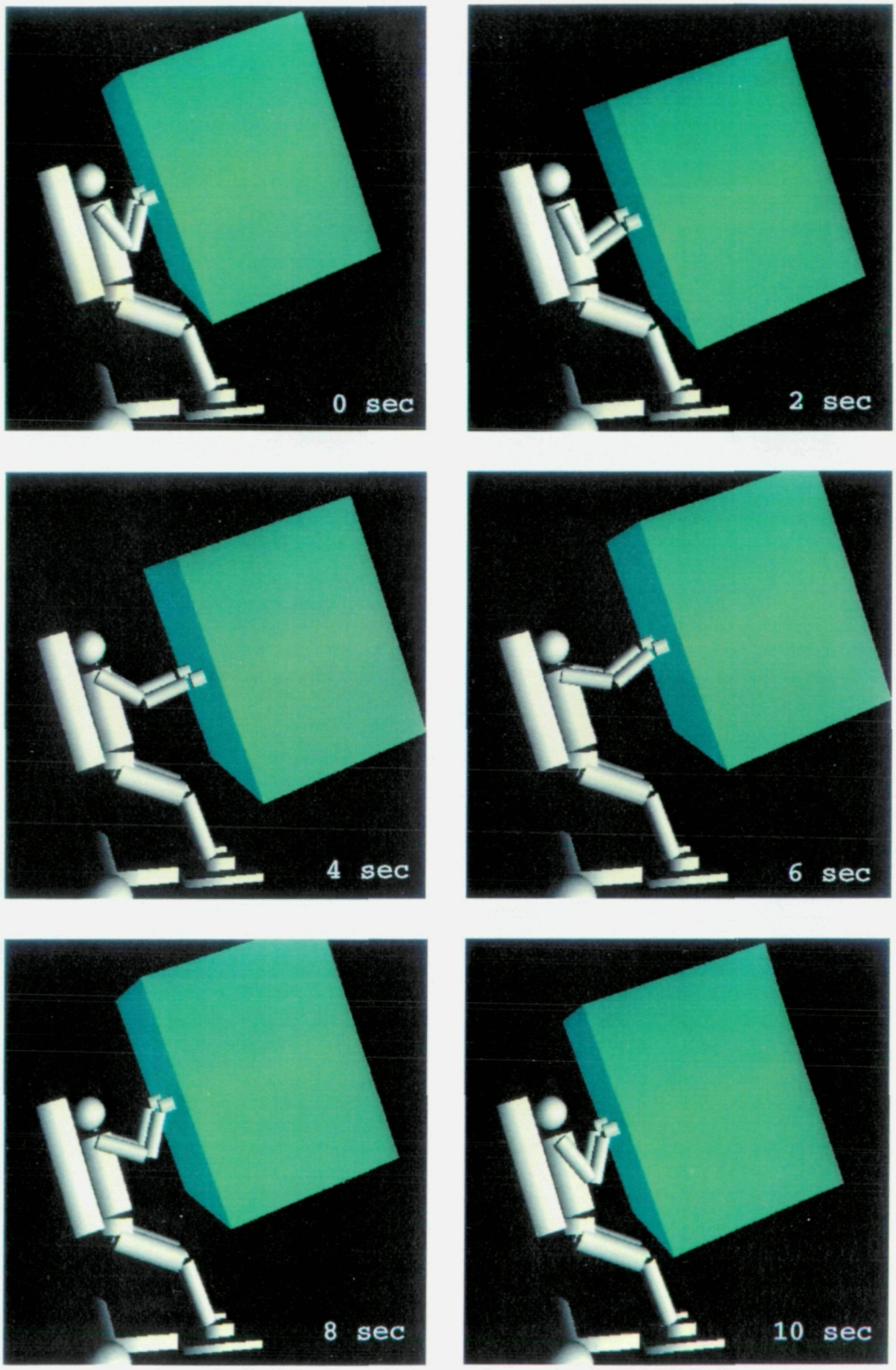

Figure 3.1 Animation sequence for simulation no. 1 – fixed lower body. Intervals are 2 seconds.

ORIGINAL PAGE
COLOR PHOTOGRAPH

3.2.1 Inverse Kinematics (No. 1 - Fixed Lower Body)

The first category of data, namely, joint angles, is presented in Figure 3.2. The limits on joint range of motion were obtained from the listings for the EMU (Shuttle spacesuit) mobility in the NASA "Man-Systems Integration Standards" (NASA-STD-3000) publication (NASA 1987). The range of motion values are summarized in Table 3.3. In general, the values were calculated by taking the average between the 5th and 95th percentile values which were originally derived from measurements on a statistically large population of test subjects. The exception to this method was the wrist joint, for which spacesuit data was not available for the particular joint axis desired (wrist radial and ulnar deviation). Wrist values were calculated by taking 85% of the unsuited (shirt sleeve environment) values listed in the same reference. The fraction of 85% was used because this is the general estimated mobility for the EMU, which was also obtained from NASA-STD-3000.

Table 3.3 EMU joint range of motion limits (edited from NASA-STD-3000).

Joint	Lower Limit [deg]	Upper Limit [deg]
Ankle	-40.0	40.0
Knee	0.0	120.0
Hip	-70.0	0.0
Shoulder	0.0	180.0
Elbow	0.0	130.0
Wrist	-28.3	22.8

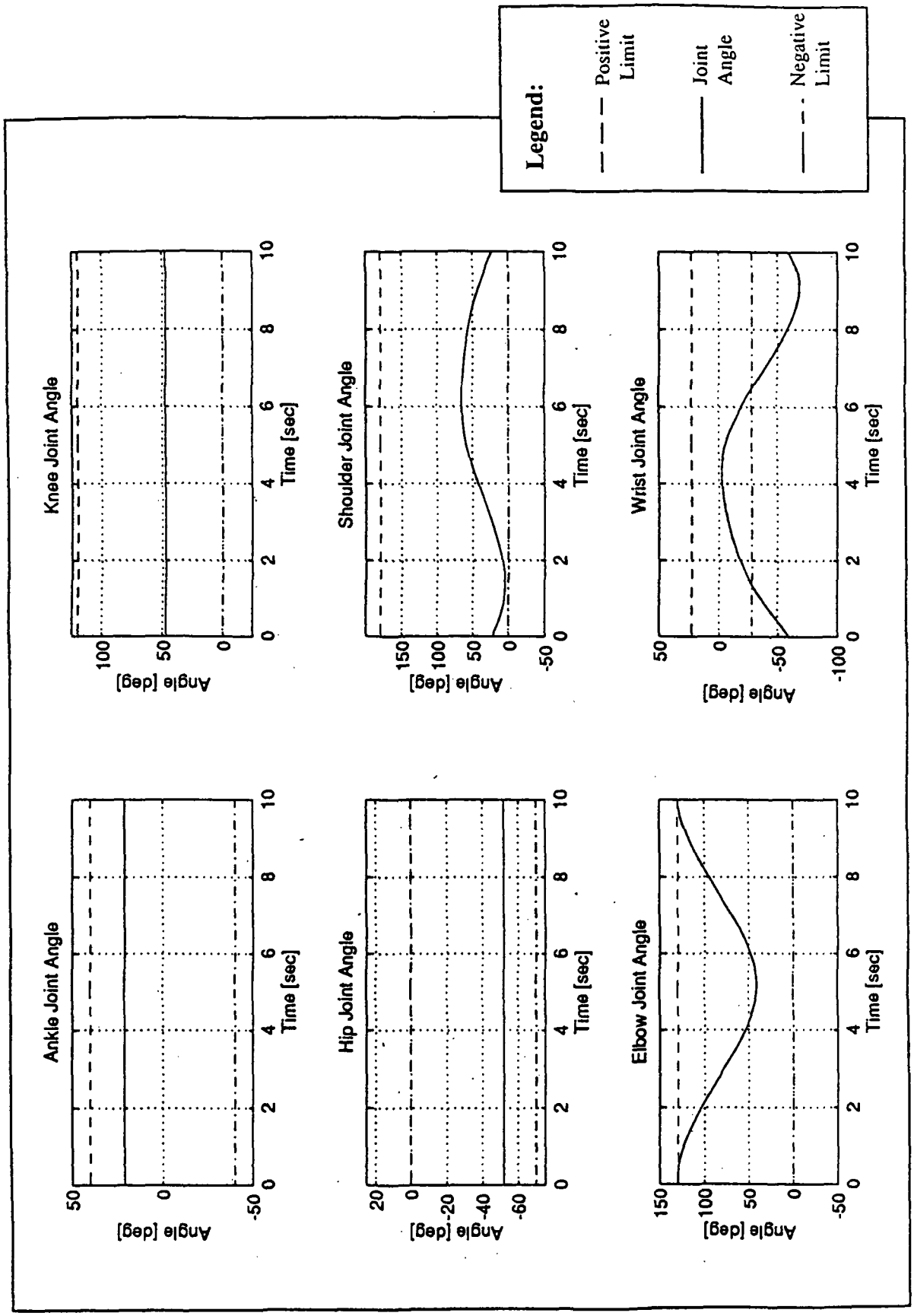

Figure 3.2 Joint angle plots for simulation no. 1 (fixed lower body).

As expected, the first three plots in Figure 3.2 confirm that the joint angles of the ankle, knee, and hip, remain fixed at the initial values of 21°, 47°, and -52° respectively. This is exactly what was intended since these joints were prescribed to remain at these angles throughout this particular simulation run.

The shoulder, elbow, and wrist plots are more interesting. The shoulder joint data follows a roughly sinusoidal trend. It starts at and returns to a value of 29°. Again, this is as expected since the hand c.m. describes a closed circle. The maximum and minimum angles reached in the three articulated joints are summarized in Table 3.4. Note that the term "minimum" refers to the lower of the two values on a signed scale so that a negative angle is called a "minimum" even if its absolute magnitude is larger than a "maximum" positive value. This convention is also followed for the velocity, acceleration, and torque parameters.

Table 3.4 Maximum and minimum angles reached by articulated joints during simulation No. 1 - Fixed Lower Body.

Joint	Time of Max. [sec]	Max. Angle [deg]	Time of Min. [sec]	Min. Angle [deg]
Shoulder	6.20	65.1	1.35	4.9
Elbow	0.00 & 10.00	130.0	5.15	40.4
Wrist	4.25	-2.9	9.10	-67.9

By observing the limiting curves for joint range of motion, it can easily be seen that the wrist is the only joint exceeding its range of motion. In this case, however, the excursions below the lower limit of -28.3° are so severe, the maximum deviation is -49.8°, the task becomes completely impossible. Changes incorporated in the second simulation sought to avoid this problem.

Values of joint velocity are displayed in Figure 3.3. As expected the ankle, knee, and hip joints exhibit zero velocity since their angles are fixed. The range of values attained by the remaining three joints are shown in Table 3.5. No limits are shown on the plots in Figure 3.3 because no data has been found on the limits of human joint velocity in a spacesuit.

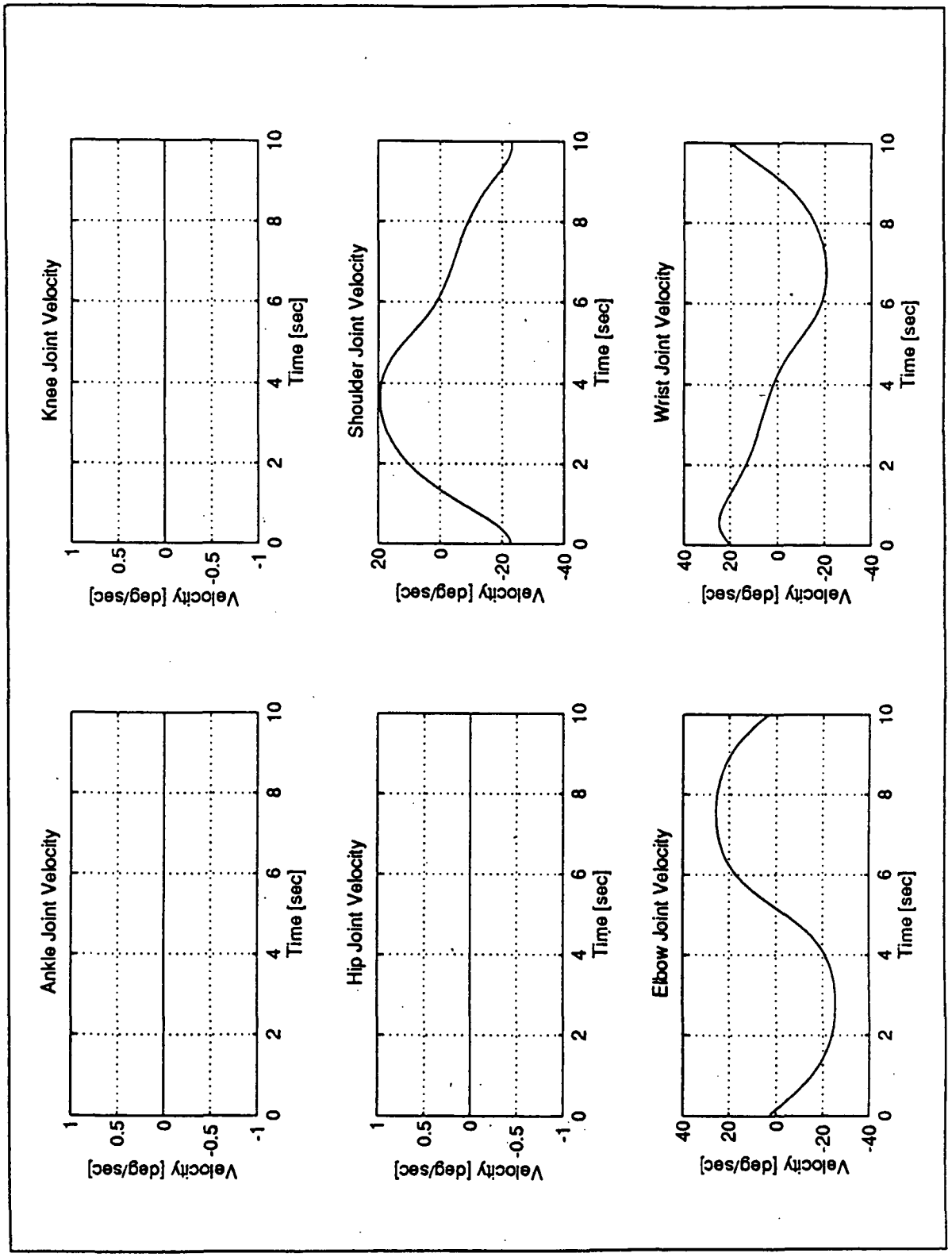

Figure 3.3 Joint velocity plots for simulation no. 1 (fixed lower body).

Table 3.5 Maximum and minimum velocities for articulated joints during simulation No. 1 - Fixed Lower Body.

Joint	Time of Max. [sec]	Max. Velocity [deg/sec]	Time of Min. [sec]	Min. Velocity [deg/sec]
Shoulder	3.65	19.4	9.90	-23.2
Elbow	2.80	-25.4	7.55	25.4
Wrist	0.55	24.5	6.75	-20.5

A quick check of the velocity data is available by comparing the velocity curves with the joint angle curves. It is observed that the joint velocity curves do in fact represent the derivative of the joint angle curves as expected.

The last data set that falls under the description of inverse kinematics, are the joint acceleration curves shown in Figure 3.4. Once again the ankle, knee and hip joints are fixed. The shoulder, elbow, and wrist joint acceleration curves are the first derivatives of the corresponding velocity curves and attain the extreme values shown in Table 3.6. Again, no data has been obtained on the limits of joint acceleration for a person wearing a spacesuit. In the case of acceleration, however, it would seem that these limits would be of little value, particularly since the mechanical properties of a spacesuit appear to depend primarily on joint angle (torsional spring force), with possibly some lower level forces from damping (velocity dependence). At any rate, since joint acceleration is related to joint torque, the limits on human strength, displayed along with the joint torque values, provides an indication as to whether acceleration values are realistic.

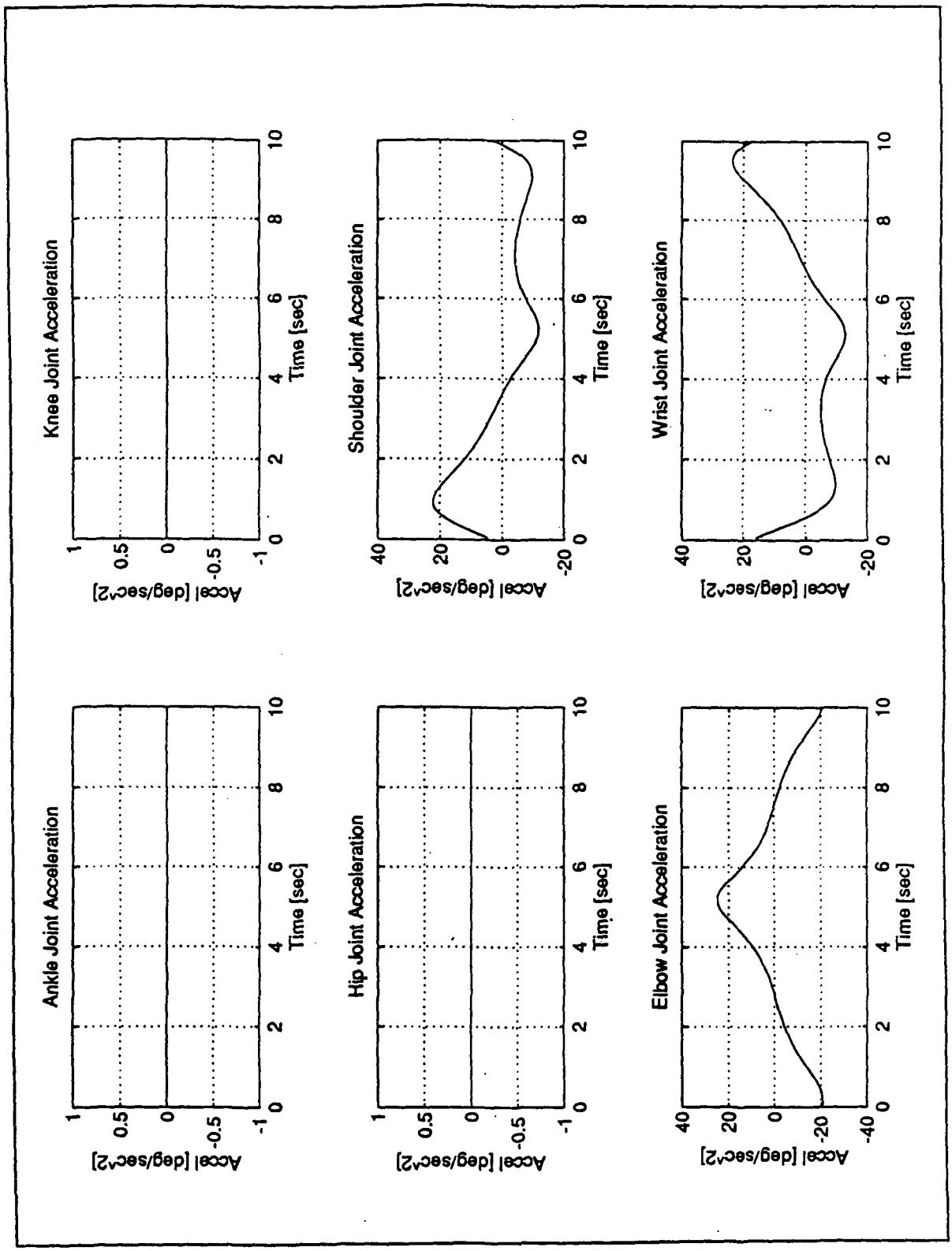

Figure 3.4 Joint acceleration plots for simulation no. 1 (fixed lower body).

Table 3.6 Maximum and minimum accelerations for articulated joints during simulation No. 1 - Fixed Lower Body.

Joint	Time of Max. [sec]	Max. Acceleration [deg/sec^2]	Time of Min. [sec]	Min. Acceleration [deg/sec^2]
Shoulder	0.95	22.1	5.20	-11.9
Elbow	5.15	24.6	0.15	-20.9
Wrist	9.50	23.6	5.10	-12.8

3.2.2 Inverse Dynamics (No. 1 - Fixed Lower Body)

Values of joint torque, obtained from the inverse dynamics phase of the first simulation, are displayed in Figure 3.5. In this case, the curves of the system joint torques reveal fairly smooth sinusoidal shapes. The biggest difference between this family of plots and those in the inverse kinematics section is the fact that the ankle, knee, and hip joints now exhibit non-zero and non-stationary values. Non-zero torques should be expected because even though the joints maintain a constant position, they must exert varying amounts of torque to hold that position as the configuration and torques in the rest of the system change. One might think of these torques as reaction torques. The maximum and minimum values reached by the system torque curves are listed in Table 3.7.

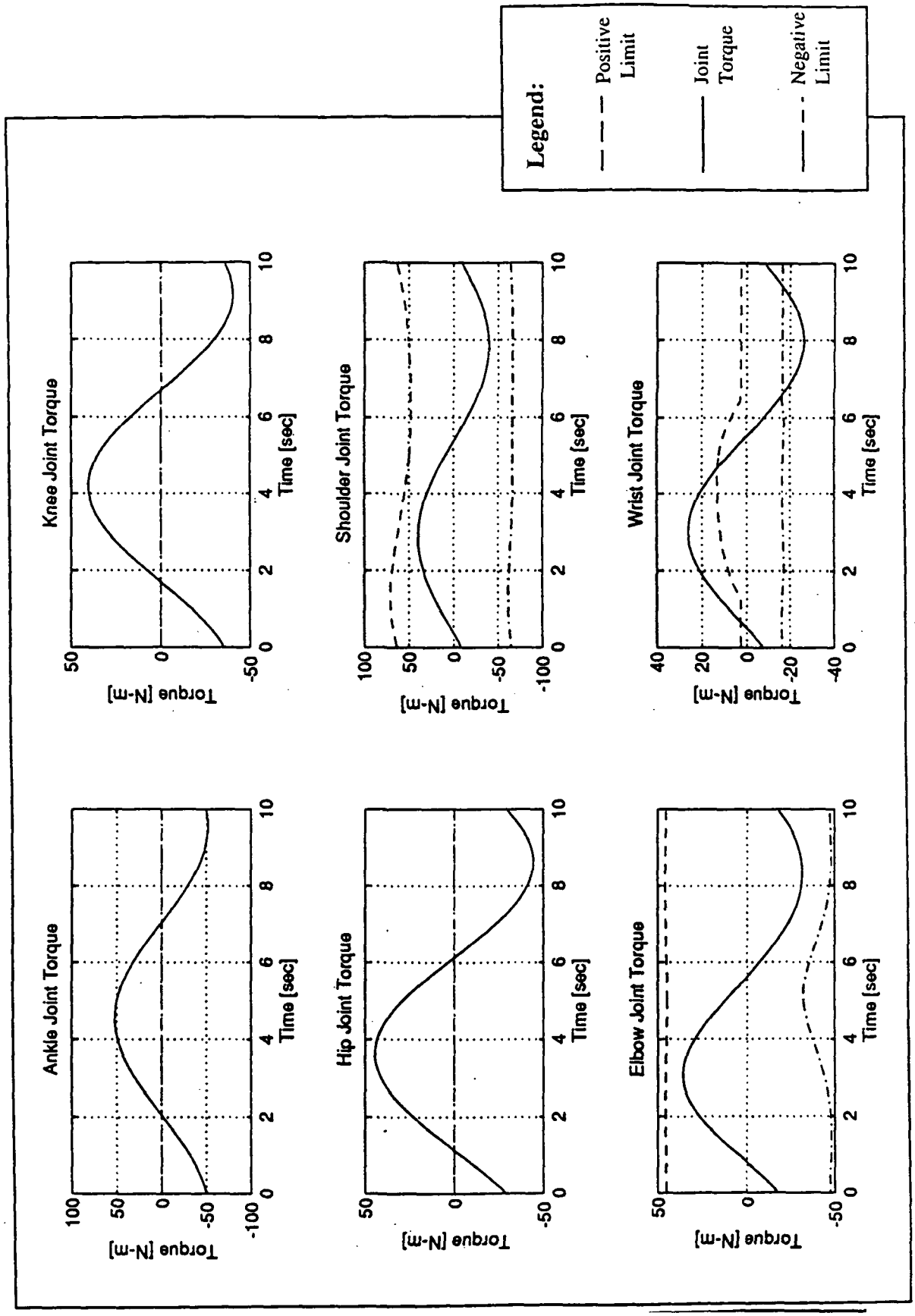

Figure 3.5 Joint torque plots for simulation no. 1 (fixed lower body).

Table 3.7 Maximum and minimum torques reached by system joints during simulation No. 1 - Fixed Lower Body.

Joint	Time of Max. [sec]	Max. Torque [N-m]	Time of Min. [sec]	Min. Torque [N-m]
Ankle	4.55	52.0	9.55	-51.8
Knee	4.20	40.5	9.20	-40.3
Hip	3.65	44.6	8.65	-44.5
Shoulder	2.85	39.9	7.85	-39.9
Elbow	3.05	36.0	8.30	-31.8
Wrist	3.00	26.1	8.00	-26.1

Three interesting facts surface upon surveying the values in this table. Firstly, all of the joints with the exception of the elbow joint, exhibit maxima and minima that are exactly 5.00 seconds apart (half of the total simulation time). The time between the maximum and minimum torque values for the elbow joint is a slightly larger value of 5.25 seconds. Secondly, all of the joints with the exception of the elbow joint, have a maximum and minimum torque value that are symmetrical around zero Newton-meters. The elbow joint average torque is slightly offset from zero at a value of 4.25 N-m. Thirdly, it is clear that the ankle joint experiences the highest torque values in both positive and negative senses, which is not too surprising since the ankle joint is related to the object being manipulated, and thus to the endpoint force exerted, by the longest moment arm in the body. Furthermore, the ankle is not assisted in providing reaction torques by the weight of the astronaut's body, as would be the case in a one-g environment.

3.3 Simulation No. 2 - Compliant Lower Body

The second simulation is an improvement on the first. Two objectives were followed during the creation of this simulation. Firstly, violations of human physiological constraints such as joint range of motion and torque were avoided, and secondly, additional features were incorporated into the simulation to make the results more realistic than those obtained in the first simulation.

The most significant concern that came out of an observation of the results from the first simulation was the deviation of the wrist joint from its allowable range by a very large amount. To avoid this problem, the initial configuration of the astronaut was altered slightly. The ankle, knee, and hip joint were set to the same neutral body posture angles as before (21°, 47°, and -52°). This time, however, the shoulder joint was set to an initial

angle of 0°; the elbow joint was set to an initial angle of 90°; and the wrist joint was set to an initial angle of 0°. This means that the wrist starts off in a comfortable position close to the center of its range of motion. The initial configuration for this simulation can be seen in Figure 3.12.

To reduce the large joint torques observed in the first simulation, the angular velocity with which the hand c.m. traces out the circular trajectory was reduced to half of the value of the first simulation so that the circle is completed in 20 seconds instead of 10 seconds. Initially, the simulation was attempted with the same radius as before (0.15 m). Unfortunately, due to the new starting position, the arm ran into a singular configuration (full extension) because part of the circle lay outside of the reach envelope of the c.m. of the hand. To avoid this condition, the radius of the circular trajectory was reduced to 0.75 m. This also helped to reduce the required joint torques as explained below.

Instead of fixing the ankle, knee, and hip joints, torsional springs and dampers were added to these joints to provide some passive compliance. It is a reasonable approximation to model the passive impedance of these joints in this way since it is well known that muscle actuators exhibit the gross mechanical properties of both elasticity and damping (McMahon 1984). In a way, these springs and dampers act like proportional-plus-derivative controllers which try to maintain their respective joints at the desired angles by exerting torque proportional to the angular deviation of the joint from the desired angle (spring) and proportional to the angular velocity of the joint (damper) according to the relation

$$\tau_{\text{joint}} = -k_{rot}\left(q_{\text{joint}} - q_{\text{bias}}\right) - b_{\text{damp}}\dot{q}_{\text{joint}} \tag{3.1}$$

where

τ_{joint} = passive torque exerted on joint
k_{rot} = spring constant in N - m / deg
q_{joint} = joint angle measured from reference position
q_{bias} = joint bias angle (desired position)
b_{damp} = damping constant
$\dot{q}_{\text{joint}}$ = joint angular velocity

An equation of this form is applied to each of the ankle, knee, and hip joints. Based on estimates of the order of magnitude of human joint torque strength, k_{rot} was chosen to be 100 N-m/rad and b_{damp} was chosen to be 10 N-m/(rad/sec) for all three joints. In addition,

each of the three joints are provided with very stiff "joint stop" springs (k_{rot} = 1000 N-m/rad) that are activated if the joint angle exceeds its limits.

The hand is prescribed to remain at the orientation of its initial configuration (w.r.t. ground) so that the orientation of the Spartan payload remains fixed and it executes only translational motions. The elbow and shoulder are allowed complete freedom in following the prescribed endpoint trajectory, as in the first simulation. The logic behind the choice of conditions described above, including the placement of springs and dampers, is that the astronaut uses his lower body in a passive way, in an attempt to maintain a certain posture, while he uses his arms to move the payload along the desired trajectory. The wrist joint is used to keep the payload at a fixed orientation.

As with the first simulation, the sequence of motions visualized in the animation of simulation no. 2 are shown in the six image composite of Figure 3.6. The most noticeable difference between the animation of this simulation and the animation of the first simulation is that the astronaut's body sways back and forth as the object is being manipulated. At first the astronaut's body tilts backward, mainly due to ankle extension, in reaction to the force he exerts on the payload as he pushes it away from his body. As the payload reaches the furthest point from his chest (halfway point in trajectory), his body tilts forward, mainly due to ankle flexion, in reaction to the force with which he pulls the Spartan payload toward his body.

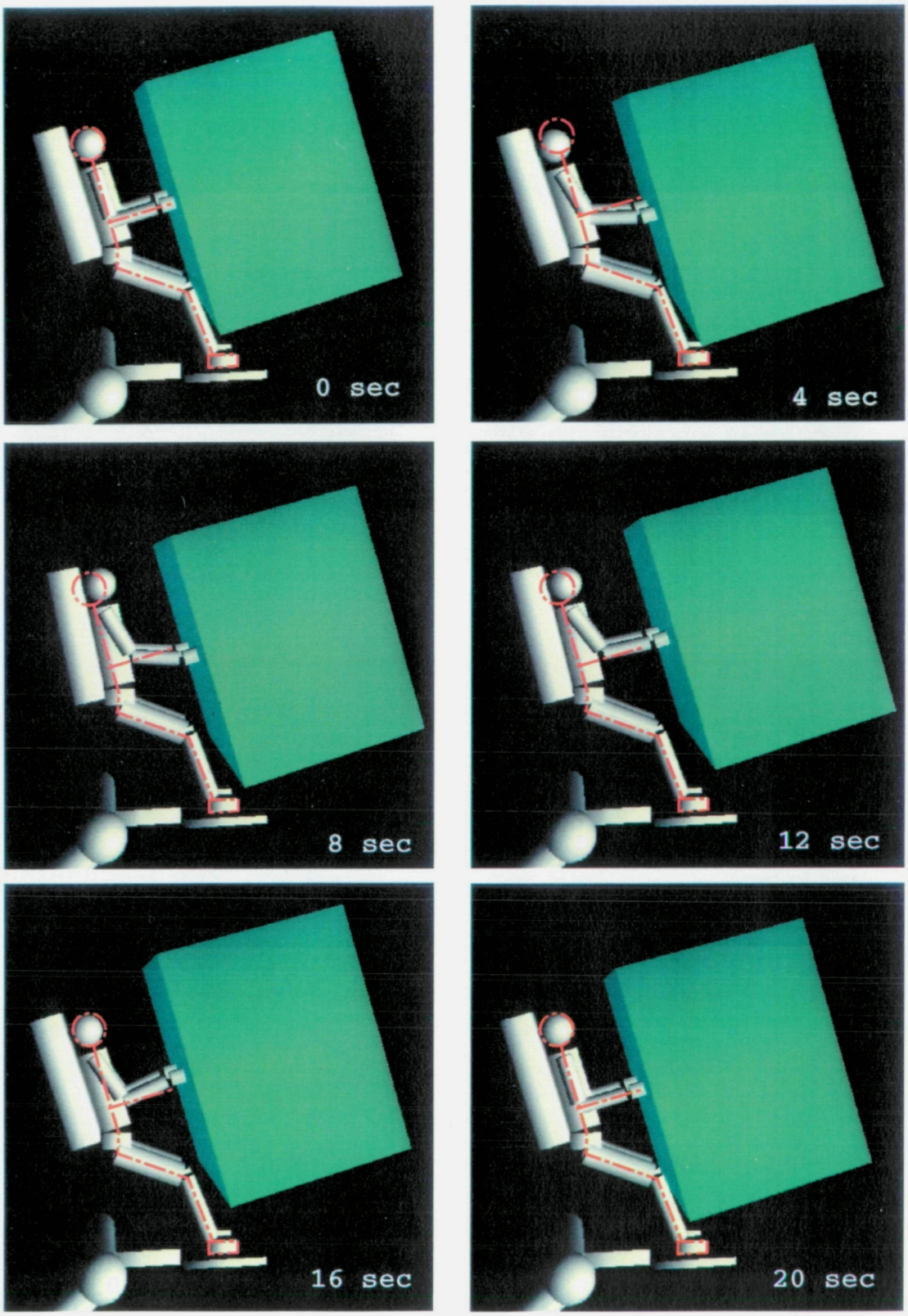

Figure 3.6 Animation sequence for simulation no. 2 – compliant lower body. Intervals are 4 seconds. Red dashed lines indicate starting configuration of body to accentuate lower body motions..

ORIGINAL PAGE
COLOR PHOTOGRAPH

3.3.1 Inverse Kinematics (No. 2 - Compliant Lower Body)

Values of joint angle are revealed in the plots shown in Figure 3.7. Maxima and minima for each joint angle are summarized in Table 3.8. The first noticeable difference between this simulation and the previous one is that the lower body joints (ankle, knee, and hip) are no longer stationary. Instead, they execute small oscillations around their starting angles. An important difference in the second simulation is that the wrist angle time history is entirely contained within the range of motion limits. All of the other joint angles are contained within their range of motion limits, except for a slight dip below the lower limit of the shoulder joint. This violation could easily be remedied by either starting the shoulder joint at a slightly positive initial angle or by incorporating stiff spring joint-stops in the shoulder.

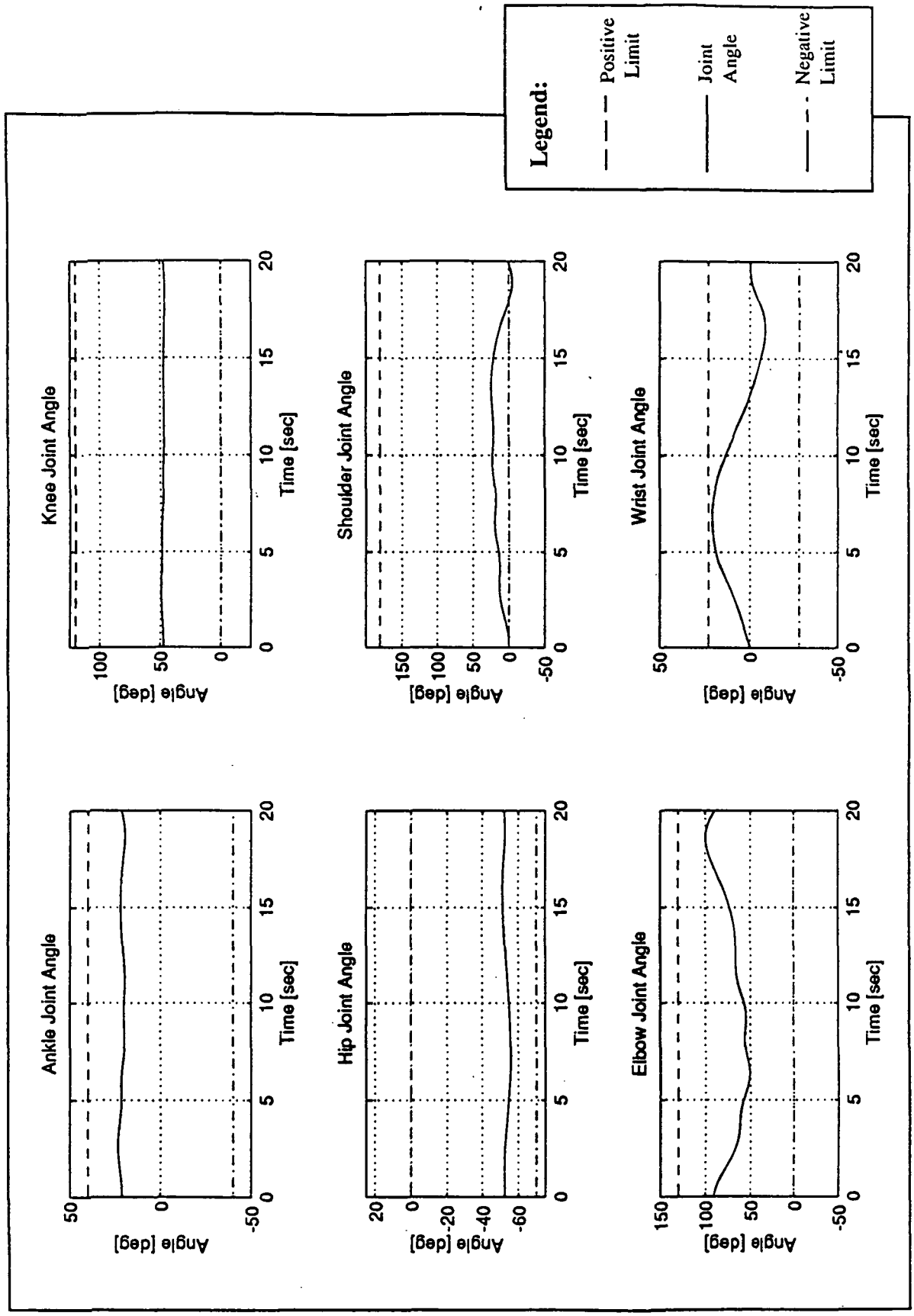

Figure 3.7 Joint angle plots for simulation no. 2 (compliant lower body).

Table 3.8 Maximum and minimum angles reached by articulated joints during simulation No. 2 - Compliant Lower Body.

Joint	Time of Max. [sec]	Max. Angle [deg]	Time of Min. [sec]	Min. Angle [deg]
Ankle	2.75	23.13	18.65	19.43
Knee	3.05	49.23	18.45	46.04
Hip	15.95	-51.14	7.15	-55.69
Shoulder	13.65	25.06	18.95	-4.82
Elbow	18.55	99.66	6.45	50.92
Wrist	6.85	20.72	16.55	-9.26

Angular velocity values for the various joints are plotted in Figure 3.8. The summary of maxima and minima for joint velocities is given in Table 3.9. The velocity values for the ankle, knee, and hip exhibit small fluctuations around an approximate mean of 0 deg/sec. The initial oscillations that last for the first half of the simulation period are accounted for by the sudden start of the manipulation task causing abrupt peaks in acceleration at the beginning of the simulation (seen in the acceleration plots of Figure 3.9). The velocity oscillations gradually die down due to the slight damping in the lower body joints.

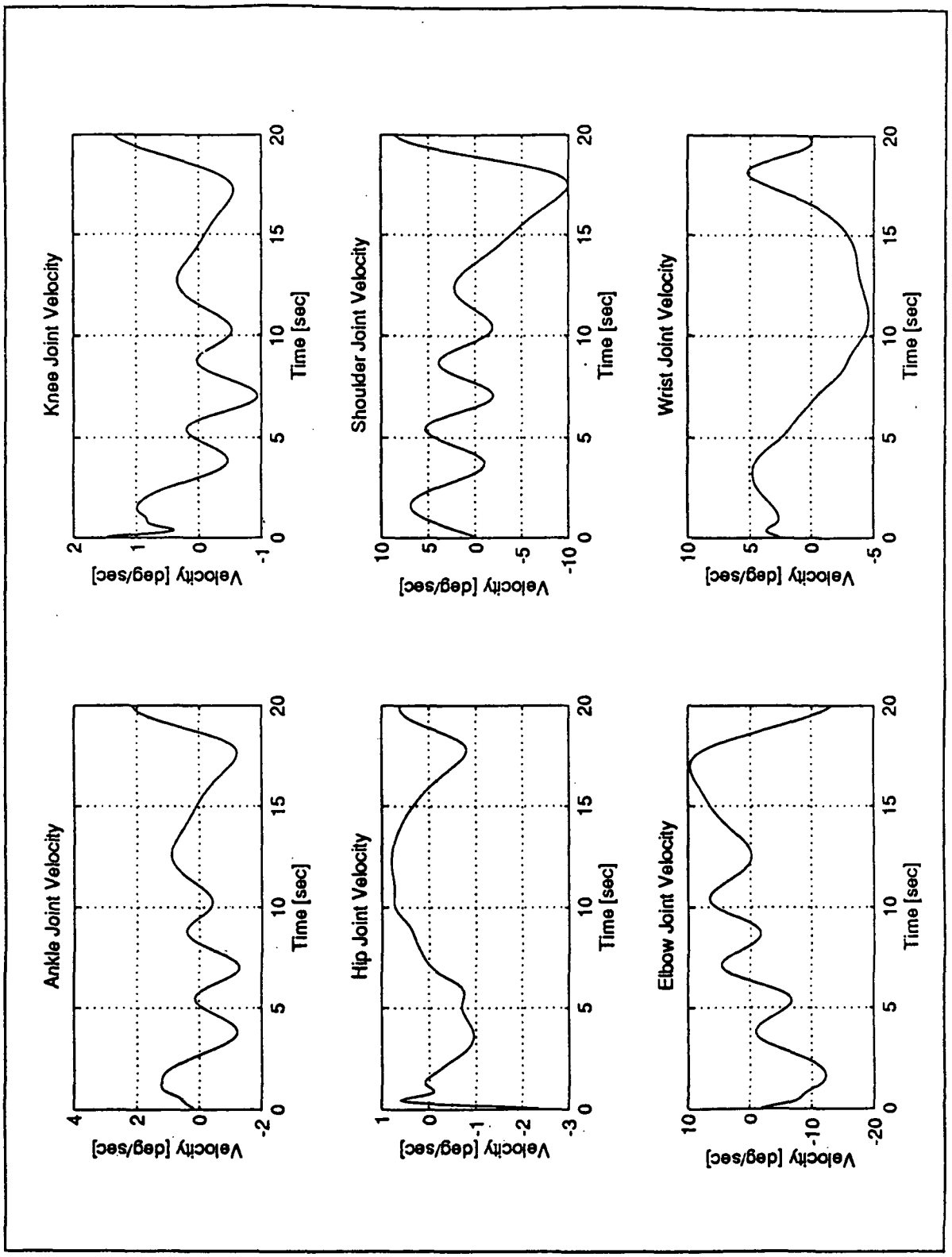

Figure 3.8 Joint velocity plots for simulation no. 2 (compliant lower body).

Table 3.9 Maximum and minimum velocities for joints during simulation No. 2 - Compliant Lower Body.

Joint	Time of Max. [sec]	Max. Velocity [deg/sec]	Time of Min. [sec]	Min. Velocity [deg/sec]
Ankle	20.00	2.29	7.05	-1.15
Knee	20.00	1.15	7.00	-1.15
Hip	12.30	0.57	0.10	-1.72
Shoulder	20.00	8.59	17.50	-9.74
Elbow	17.00	9.74	20.00	-13.18
Wrist	18.10	5.16	11.00	-4.58

The acceleration plots, displayed in Figure 3.9, show that the lower body joints experience slight acceleration, although usually on a smaller scale than the arm joints. All of the joint accelerations fluctuate around a zero mean. Most of them also exhibit a sharp acceleration spike at the beginning of the simulation run, as mentioned above, caused by the discontinuity in velocity at the beginning of the manipulation task. These spikes cause oscillations, but they appear to dissipate by the time the simulation is into the second half of its run time due to the damping in the lower body joints. The joint torque curves for the arm joints are much smoother (almost sinusoidal) than the lower body joints due to the smoothing effect of the linearized least squares solver applied to these joints during the inverse kinematics phase and because these joints are not controlled by springs and dampers. The maximum and minimum acceleration values are summarized in Table 3.10.

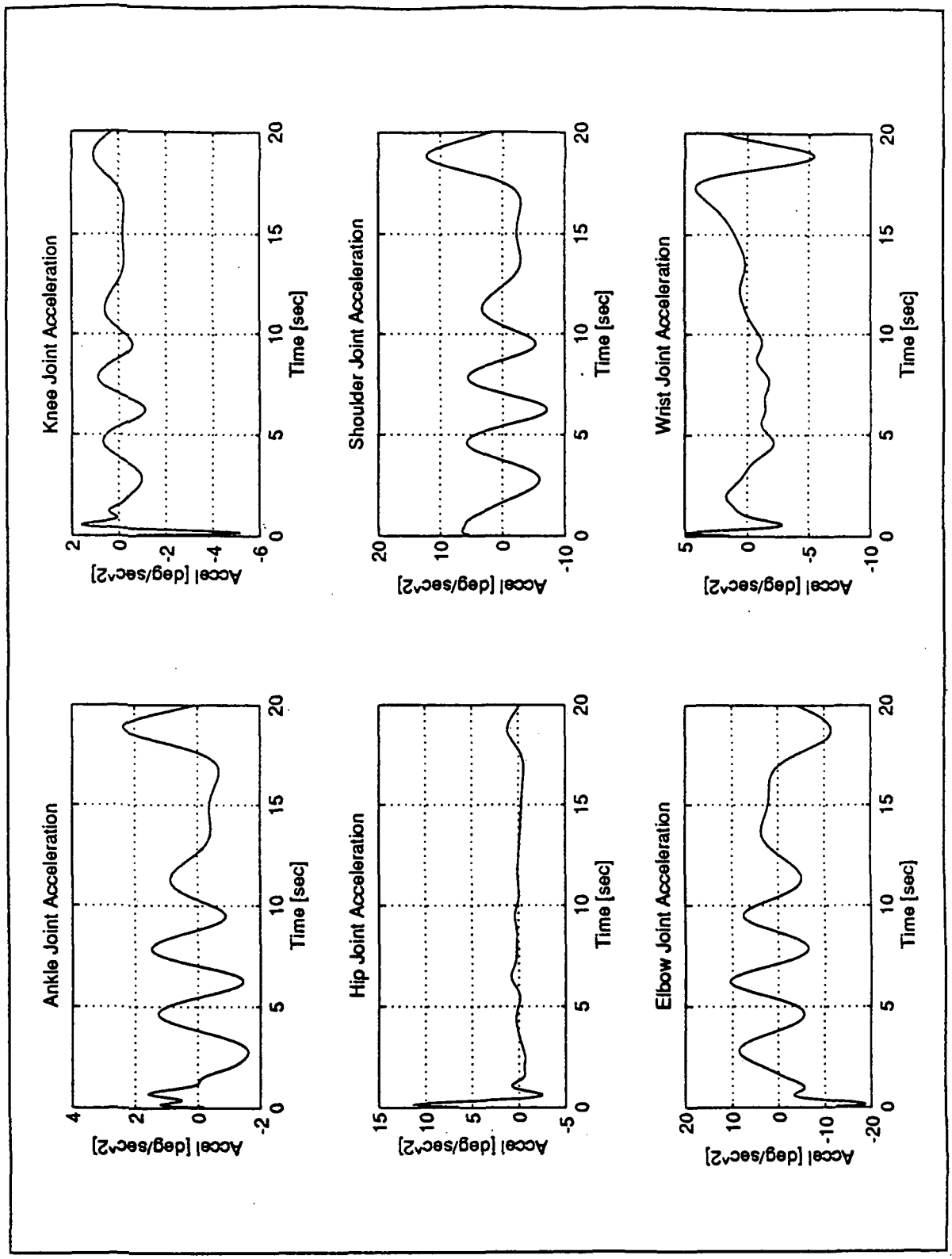

Figure 3.9 Joint acceleration plots for simulation no. 2 (compliant lower body).

Table 3.10 Maximum and minimum accelerations for joints during simulation No. 2 - Compliant Lower Body.

Joint	Time of Max. [sec]	Max. Acceleration [deg/sec^2]	Time of Min. [sec]	Min. Acceleration [deg/sec^2]
Ankle	18.90	2.29	2.70	-1.72
Knee	0.50	1.72	0.20	-4.58
Hip	0.20	10.89	0.60	-2.29
Shoulder	18.80	12.03	6.20	-6.88
Elbow	6.20	10.31	0.20	-18.33
Wrist	0.20	4.58	18.90	-5.16

3.3.2 Inverse Dynamics (No. 2 - Compliant Lower Body)

Joint torque values for the second simulation are shown in Figure 3.10 and the maximum and minimum values are summarized in Table 3.11. A dramatic reduction in torque magnitude is demonstrated for all the joints as compared to the first simulation. Clearly, the speed with which the endpoint trajectory is followed has a large effect on the required joint torques. On average, the magnitudes of the torque values are about one eighth to one tenth of the magnitudes of the torques obtained in the first simulation. The angular velocity at which the circular path is traced out was reduced by one half and the circle radius was reduced by one half so the torque factor of one eighth is approximately predicted by the simple relation

$$f = m\omega^2 r \tag{3.2}$$

where

f = centrifugal force
m = mass of manipulated payload (Spartan)
ω = angular velocity of circular trajectory
r = radius of circle

Since the moment arms over which the centrifugal force (applied at the hand) acts, in relation to the various segments of the system, do not vary to a great extent, the resulting joint torques are approximately proportional to the magnitude of the centrifugal force during both simulations and are thus also approximately scaled by the factor of one eighth.

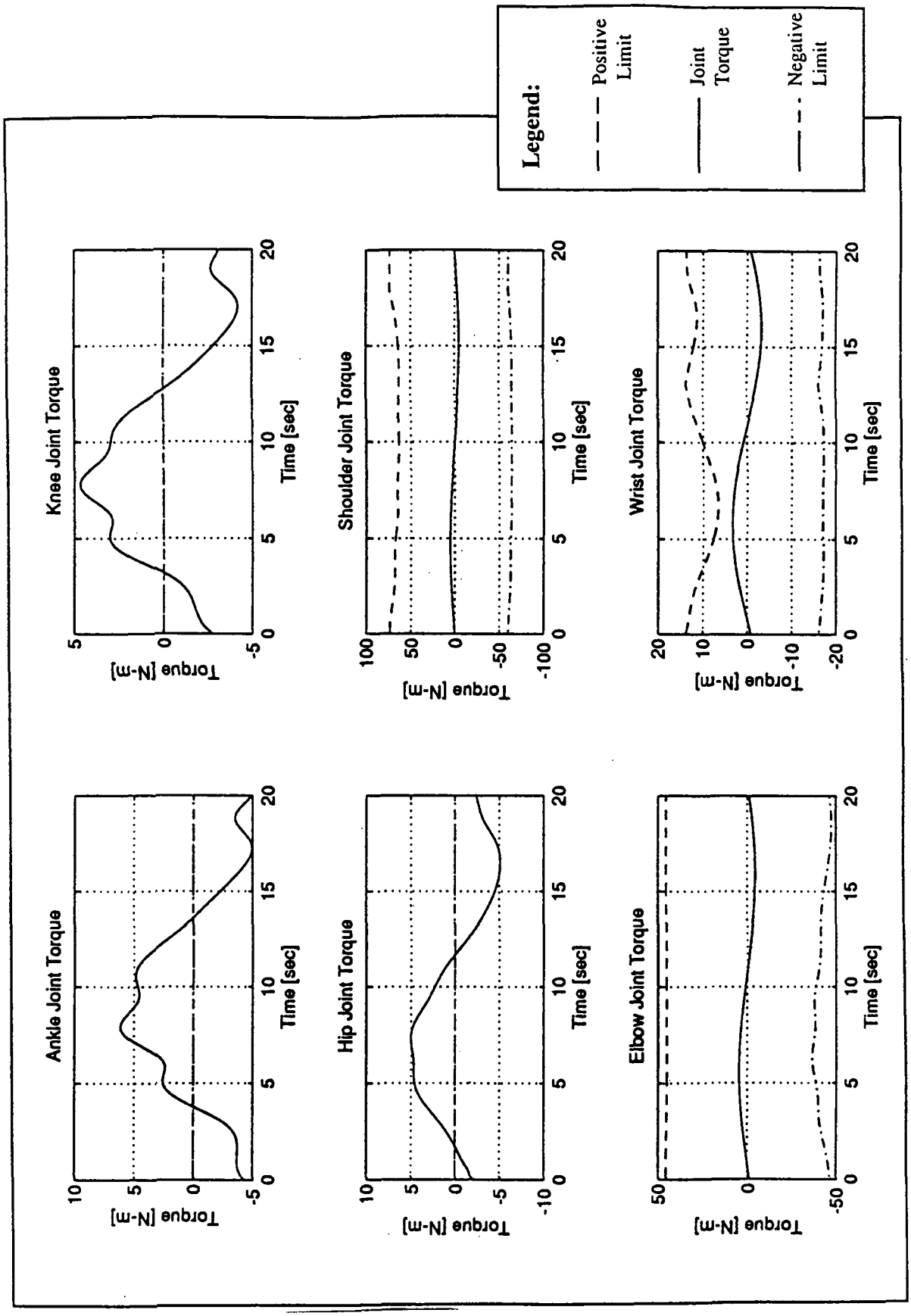

Figure 3.10 Joint torque plots for simulation no. 2 (compliant lower body).

Table 3.11 Maximum and minimum torques for joints during simulation No. 2 - Compliant Lower Body.

Joint	Time of Max. [sec]	Max. Torque [N-m]	Time of Min. [sec]	Min. Torque [N-m]
Ankle	8.00	6.14	17.30	-4.95
Knee	7.80	4.68	17.10	-4.19
Hip	7.30	5.01	16.50	-5.13
Shoulder	4.80	5.04	15.00	-5.14
Elbow	5.50	4.45	16.00	-4.50
Wrist	5.80	3.26	15.80	-3.26

As seen in Figure 3.10 the large reduction in joint torques places this manipulation task within the range of human strength values for the various joints. This fact, combined with the observation that the range of motion of the joints are not significantly exceeded, predicts that the mass manipulation task evaluated in the second simulation can quite comfortably be performed by an astronaut, in contrast to the first simulation's mass handling task, which was well beyond the range of human capability.

Even though the overall joint torques have been greatly reduced, it can be seen that the largest positive torque value occurs in the ankle joint, just as in the case of the first simulation, although slightly larger negative torques occur in the hip and shoulder than in the ankle during this compliant lower body simulation.

3.4 Animation and Data Display

The animation and data display capabilities of the EVADS program are particularly successful. Even though the program is in a rudimentary stage, it has already proven invaluable in interpreting simulation results and in diagnosing problems, especially during the early stages of a simulation.

To visualize the computer representation, consider the two computer screen images shown in Figure 3.11 which were taken at the start of the first simulation. Two similar images for the second simulation are shown in Figure 3.12. One can see at a glance whether the initial configuration corresponds with that desired. If the simulation runs into a snag, such as a singularity, then the configuration causing the singularity is easily identified. In addition, the ability to correlate the animation figure with the data for a given parameter at a specific point in time, along with the availability of the whole time history of that parameter, is very useful in diagnosing the reasons for certain parameters

reaching or exceeding the limits of their nominal range (e.g., a joint angle compared to its physiological range or a joint torque compared to a human strength curve).

The three primary portions of the EVADS display, the animation area, the data plot area, and the parameter selection buttons are shown in Figures 3.11 and 3.12. Two screen images are shown, each one displaying a different viewing angle. Through the use of the pan, rotation, and zoom controls of EVADS, the user can obtain an unlimited number of different viewing angles and scales quite easily. This proves to be particularly useful when certain objects are obscured or when it is desirable to focus in on a specific detail of the animated figure.

The differences between the initial configuration for the two simulations can be noticed by comparing Figures 3.11 and 3.12. In Figure 3.11 the lower body is placed in a neutral weightlessness posture and the hands start out from a point close to shoulder level. In the initial configuration of the second simulation, shown in Figure 3.12, the lower body joints (ankle, knee, and hip) start out in the same neutral body posture, but the arm joint angles are significantly altered. The shoulder joint starts out at zero degrees (i.e., straight down along the side of the trunk), the elbow joint starts at a ninety degree angle, and the wrist joint starts out at zero degrees. All of these angles are measured with respect to the centerline of the preceding body (the shoulder angle is offset by 180° with respect to the trunk so that 0° is with the upper arm pointing down instead of up). Most importantly, it is clear that in the second simulation the wrist joint begins the mass handling task in a more comfortable position close to the center of its range of motion.

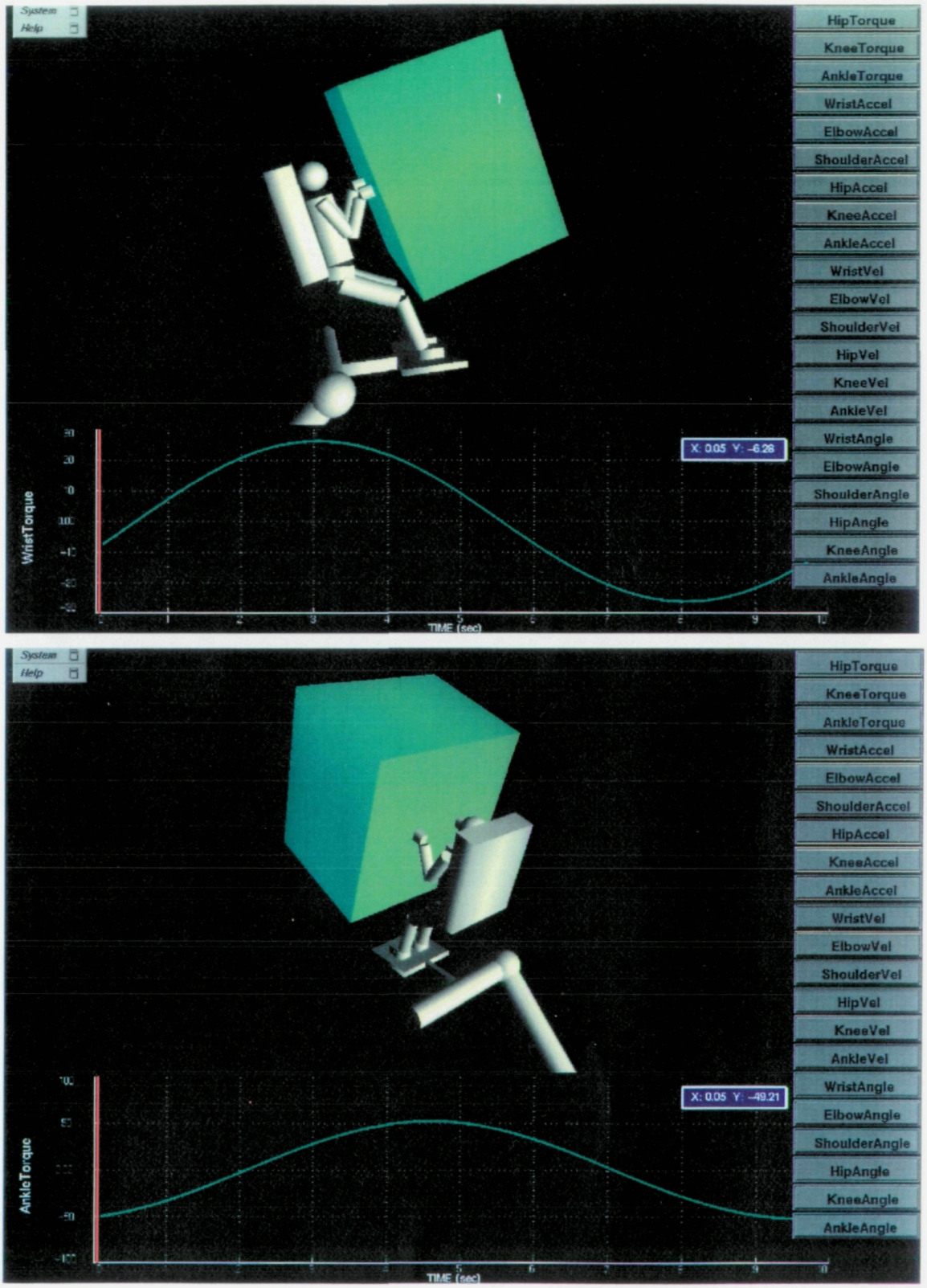

Figure 3.11 Two images of EVADS screen showing different viewing angles of simulation no. 1 – fixed lower body.

ORIGINAL PAGE
COLOR PHOTOGRAPH

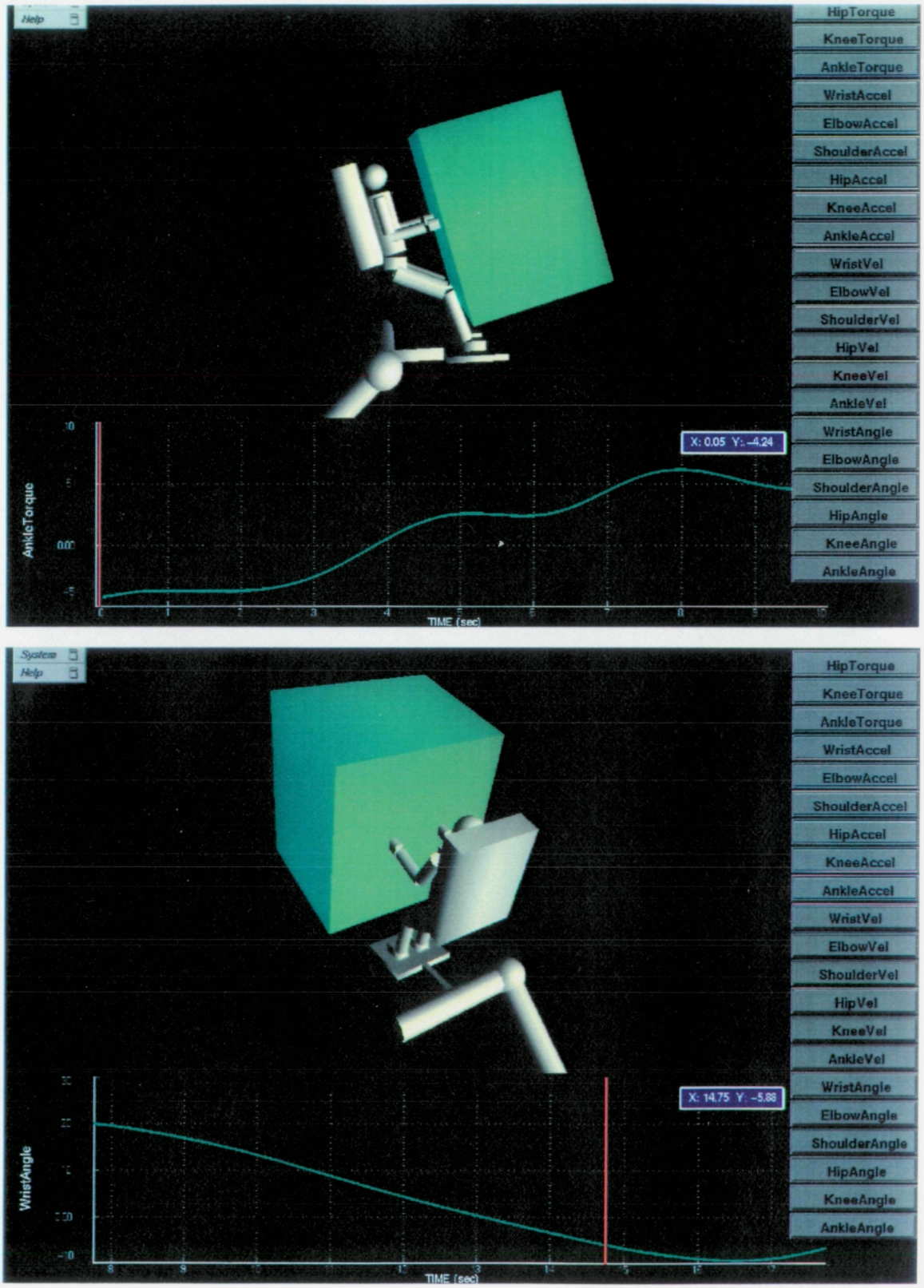

Figure 3.12 Two images of EVADS screen showing different viewing angles of simulation no. 2 – compliant lower body.

ORIGINAL PAGE
COLOR PHOTOGRAPH

4. Discussion and Conclusions

Results of this research effort have been very encouraging. It has been shown that computational simulation of extravehicular activity can overcome many of the limitations of physical simulators and at the same time reveal quantitative information on the dynamic state of the astronaut's body, such as joint torques, that was previously unavailable.

To a certain extent, the research effort described in this report was able to take advantage of past work conducted in other areas of application of multibody dynamics such as robotics or sport biomechanics. However, little or no multibody dynamics analysis has been applied to EVA and so it has been a pioneering effort in many ways. For this reason, the emphasis has been on creating a tool for dynamics analysis of EVA, rather than focusing too heavily on the accuracy and detail of the human body models employed. Nevertheless, an effort was made to ensure that the values obtained were realistic and reasonably accurate. For instance, using simplified models of the human body, the values for the hand calculated and computer calculated test torques are shown to be remarkably consistent, deviating by less than 0.03%. Still, certain simplifications should be acknowledged. Rudimentary pin joints replace the complexity of human body joints and mass properties of body segments are calculated from elementary geometric solids (cylinders, blocks, and spheres). In addition, some parameters, such as the lower body spring and damping constants, are estimated based on research and intuition rather than experimental data.

The philosophy adopted in creating simulations has been to start with the simplest possible model that yields non-trivial results. Once this model is working, it is expanded incrementally to incorporate more complexity and additional degrees of freedom and in the process yield more realistic and more accurate results. For instance, to simulate the Spartan mass handling EVA a simple seven segment model of an astronaut manipulating a massive payload has been created. It is assumed that the astronaut's feet are rigidly attached to an object fixed in inertial space. In an actual EVA, the astronaut's feet would most likely be clamped in a Portable Foot Restraint (PFR) attached to the Space Shuttle Orbiter via its robot arm (the Remote Manipulator System, or RMS). In reality, the PFR and RMS are not perfectly rigid and the although the Shuttle Orbiter's mass is very large it will still experience very small accelerations due to the astronaut's motions. Since the dynamic effects of the Orbiter, RMS, and PFR are secondary they have been ignored in

these simulations. The flexibility of the PFR and RMS, and the finite mass of the Orbiter, should be investigated in further research.

Two simulations are carried out, both of which are based on an actual EVA involving mass handling exercises using a Spartan 204 free flying spacecraft. While the second simulation improves on the first, there are certain elements that are common to both. For instance, the manipulation task is specified only in terms of the Cartesian coordinates of the endpoint (hand) of the system, although the kinematics of the system may be subject to certain constraints that direct the way in which the body achieves the motion task, e.g., fixing a joint angle or applying springs and dampers to joints. During the first phase, inverse kinematics, the simulation code "learns" the joint coordinate values of position, velocity and acceleration as the hand c.m. follows the prescribed circular trajectory by storing these values in a two dimensional state-time array. The hand maintains a fixed orientation with respect to "ground", ensuring that the Spartan payload remains at a constant attitude and executes only translational motions. In the second phase, inverse dynamics, the joint kinematics are recalled and used to prescribe the motion of the body and the required joint torques are calculated. The differences between the two simulations are described in the next two sections.

4.1 First Simulation - Fixed Lower Body

In the first simulation it is specified that the ankle, knee, and hip joints must maintain a constant angle for the duration of the run. For this reason, the angular velocity and acceleration of these joints are zero, although non-zero torques are required to hold the joints at the specified angles. The torque in each joint varies with time due to the changing configuration of the arm segments and payload, the motion state, and the torques applied in other joints.

The trajectory followed by the c.m. of the hand is a circle of radius 0.15 m, circumscribed at an angular velocity of 0.628 rad/sec (one revolution in 10 sec). The starting point of the hand c.m. is 0.300 m from the chest and aligned with the shoulder. An undesirable consequence of this starting position and of the size of the circle is that the wrist joint severely exceeds its range of motion when the hand is positioned close to the chest.

In order to maintain the required speed while manipulating a massive object like Spartan (1,201 kg) along the circular trajectory, the body is expected to exert joint torques well beyond the range of human capability. Enhancements to avoid the wrist angle and joint torque problems are addressed in the second simulation.

4.2 Second Simulation - Compliant Lower Body

The main objectives of the second simulation are to keep the wrist joint angular excursions within the limits of the wrist range of motion; to reduce the joint torque levels such that they are below the maximum torque levels achievable by a human; and to improve the overall realism of the simulation.

To avoid the range of motion violations exhibited by the wrist joint in the first simulation, the initial configuration of the system is altered for the arm joints. In this case, the shoulder starts at an angle of 0°, the elbow at 90°, and the wrist at 0° (Recall Figure 3.12). This starting configuration works very well in keeping the wrist angles within the limits, although it does cause a very slight violation of the shoulder joint's lower angular limit near the end of the 20 second simulation.

It was seen that to manipulate the heavy payload along a circular trajectory at the speed required in the first simulation (one revolution in 10 seconds) the astronaut would have to produce joint torques well beyond physiological limits due to the high accelerations of the joints. During the second simulation, a more realistic task is attempted in which the hand's circular trajectory is executed at half the angular velocity used in the first simulation and with half the radius. Fortunately, this task requires torque levels well within the limits of human capability.

The realism is also improved by implementing compliance in the lower body through springs and dampers in the ankle, knee, and hip joints. The animation clearly shows how the astronaut's body initially swings away from the payload in reaction to the forces he exerts as he pushes the payload forward, and then swings toward the payload while pulling the payload backward close to the midway point of the trajectory. It is encouraging that the realism of the simulation was enhanced to such a large extent by the addition of passive springs and dampers in the lower body joints, especially considering that the spring and damping coefficients were estimated. It appears, though, that the spring and damping coefficients were chosen too low based on the appearance of underdamped oscillations in the system together with the fact that a human is capable of producing about four times the torque levels seen in the leg joints. To model the greater stiffness in the lower body joints in the future, higher values for the spring and damping constants should be chosen. However, more data is needed on lower body torque capability before this can be accomplished. Alternatively, a more systematic approach based on control theory applied to human motion, such as optimal control methods, should lead to interesting results.

4.3 Development of Visualization Software

4.3.1 Background

In the current simulation environment, SD/FAST generates pages and pages of numerical data that represent crucial information relating to human joint angles, torques, and limits. Rather than run the data through several analysis packages, it is extremely useful to present the results of the simulation in an intuitive format. With this in mind, the two key characteristics for data visualization of EVA simulations are:

(1) Visualization of the actual task being performed, in real time.

(2) Simultaneous display of essential parameter data from the simulation routines.

Given these two requirements and the availability of a high-powered graphics workstation, it was decided that the best approach would be to develop a 3-dimensional animation of the EVA task, and use adjacent two-dimensional plots for the SD/FAST simulation data.

4.3.2 The EVADS Program

To implement the above ideas, a data visualization program called the EVA Dynamic Simulation (EVADS) was developed on a Silicon Graphics (SGI) Indigo^2 Extreme workstation. The program loads simulation data from text data files, which are generated by the SD/FAST simulation routines; these data files are simply time-histories of simulation parameters, such as joint angles, joint limits, and joint torques. The joint angle data are then used to generate a 3-D image representing the EVA astronaut in the proper position for a specific instant of time during the simulation. Similarly, position data indicates the position of any additional objects in the scene. This 3-D scene can be manipulated by using the mouse as a virtual trackball, rotating and/or translating the scene to achieve the desired perspective.

The lower portion of the screen is devoted to a two-dimensional display of parameter data, implemented as a scrolling plot of the parameter value versus time. The particular parameter to be displayed is selected by choosing an appropriately labeled button from a list at the right of the screen and clicking the mouse on it. During the simulation, the data plot scrolls across the screen to follow the task in progress as represented in the 3-D window. Several options are available for highlighting the current value of the parameter, determined by command-line arguments to the program.

The simulation data is then "played back" in real time, so that a second of the simulation lasts precisely one second in real-world time. This produces an animation of the EVA task which corresponds physically to the actual task being performed. When not running the simulation in this "real-time" mode, the user can scroll back and forth

through the simulation to highlight interesting features on the data plot. Simultaneous 3-D animation enables quick correlation between the plotted parameter values and a particular phase of the EVA task (for example, correlation of maximum ankle torque with a specific motion made by the astronaut).

The importance of visual aspects in the ability to improve on successive simulations is clearly demonstrated through the use of the animation and data plotting functions of the EVADS user interface. It is seen that the qualitative information conveyed by the animation can be just as important as the quantitative information conveyed by the plots. Combining these two elements provides the analyst with a very powerful tool for assessing the dynamic effects of EVA operations.

A number of enhancements to the EVADS program are currently being developed. These include: the ability to display more than one curve on a parameter plot and, in particular, to display physiological limits of a parameter along with that parameter (e.g., joint torque limits); the option of displaying multiple plots at the same time so that different parameters can be compared; tracing the trajectory followed by a certain point (e.g., the center of mass of the hand); and improvements to the manner in which button menus are utilized. In addition, a longer range goal is to separate the various portions of EVADS (animation, data plots, button menus) so that each of these can be contained in a window of its own. This would greatly improve the flexibility of the display format.

Ultimately, the desire is to integrate SD/FAST, the dynamic simulation code, and EVADS into one program so that the user can specify the description of the dynamic system, the initial configuration, the trajectory or force application task, the animation, and the data plots, all by means of the convenient user interface offered by EVADS. Viewing the animation and plots of a dynamic system while the simulation code is executing offers the great advantage of the ability to diagnose errors that occur in the midst of the simulation and that sometimes even cause an interruption of the simulation.

4.3.3 Recent Developments

The EVADS software is currently being ported to an X-Windows based environment, to provide a more familiar and accessible user interface. The new interface is constructed from Motif/XToolkit widgets, to achieve the familiar look and feel of most workstation-based programs under a window manager. Additionally, the core graphics routines are being rewritten, moving from the standard Silicon Graphics GL to the new OpenInventor environment, also by Silicon Graphics. The OpenInventor API is designed for the development of C++, object-based 3D scenes with a highly intuitive object structure. This will facilitate the rapid generation of 3D objects for the animation of new

simulations, and allow users to import objects generated by commercial programs such as AutoCad and ProEngineer.

4.3.4 Future Work

Several new commercial software packages have been introduced to perform many of the tasks for which EVADS was written; these programs will be evaluated in terms of their usefulness to the current project. If one of these packages proves to be extremely useful, then the data visualization effort will be moved to the commercial system. It is possible that a combination of the existing EVADS program and the commercial software may provide the easiest path for transition between the two. Additionally, three-dimensional representations of the SD/FAST data will be tested, superimposing data on the 3D astronaut model to provide even better visual correlation between the task and calculated task parameters.

4.4 Conclusions

While the simulation code and EVADS graphical interface are clearly still in the developmental stage, it is felt that the main objectives of this stage of the research effort were accomplished. In particular, the primary goal of demonstrating the utility of computational simulation of multibody dynamic systems for EVA research and training was achieved. The specific objectives of this research effort, as listed in chapter 1, were met in the following ways.

1) A convenient means of modeling the dynamic system was demonstrated by means of the seven segment model of the astronaut and the attached payload. This model was described in a system description text file which was used as input to SD/FAST.

2) The system model was transformed into equations of motion by means of the SD/FAST program which represented these equations in an implicit computational form using C code.

3) Computer code written in C language was used to drive the desired simulations by utilizing the functions representing the equations of motion. It was shown that this simulation code is adaptable to a variety of conditions by starting the two simulations from different initial configurations and by making the lower body rigid in the first simulation and compliant in the second simulation.

4) The astronaut motion to be performed was specified in terms of task (endpoint) coordinates alone by means of two virtual sliding joints defined in the X and Y directions of the global coordinate system. The kinematics, in terms of joint coordinates, of the astronaut's body during the manipulation task were successfully calculated using only the endpoint trajectory time history as input.

5) An inverse dynamics computation was successfully performed in each simulation to determine the joint torques using the calculated joint kinematic data (angular position, velocity, and acceleration) as input.

6) A graphics program displaying animation and data plots was successfully created. This program, called EVADS, uses simulation data as input and creates animation that is synchronized with the calculated data plots at the active time point in the plot display area. The user has the ability to select which parameter is displayed, to run the animation in real time, and to step back and forth through the simulation time history.

7) The results of inverse kinematics and inverse dynamics portions of the simulations were interpreted both quantitatively and qualitatively. Consideration of the results produced conclusions about the feasibility and efficiency of the simulated EVA operation and led to practical suggestions about how the actual EVA task might be altered to improve effectiveness. Furthermore, these results gave clues as to how the simulation itself might be improved.

8) Significant improvements in realism and accuracy were accomplished by means of the refinements incorporated in successive simulations. The second simulation successfully solved the problems of wrist joint range of motion violation and unattainable joint torques while the overall realism of body motions was enhanced.

While both of the simulations performed represent highly simplified models of EVA tasks, it is encouraging that significant and revealing results are already obtained by applying the principles of multibody dynamics. Not only does computational simulation provide useful quantitative and qualitative predictions of the dynamic effects involved in

a planned EVA, but it can also facilitate the creation of practical concepts for improving the efficiency and comfort of an EVA task. A good example of this arises by observing that the largest joint torques in both simulations occurred in the ankle. Clearly, the mechanical disadvantage that the ankle joint incurs, in terms of both the overall configuration of the body and payload and in terms of its own construction (somewhat of an Achilles' Heel syndrome), is bound to be a source of weakness and inefficiency in any EVA task involving the manipulation of large masses or the exertion of large forces via the hands. The problem could be alleviated by means of a brace mechanism which provides a stiff load path between a cuff around the lower leg (just below the knee) and the Portable Foot Restraint (PFR) or some other foot restraint. The brace would have a telescoping action and pivots at the points of attachment on the lower leg and PFR to allow freedom of movement when unlocked. Turning a simple locking handle, within reach of the astronaut's hand, would rigidize the brace prior to the performance of a manipulation task. The anticipated location and conceptual design of this device is shown in Figure 4.1.

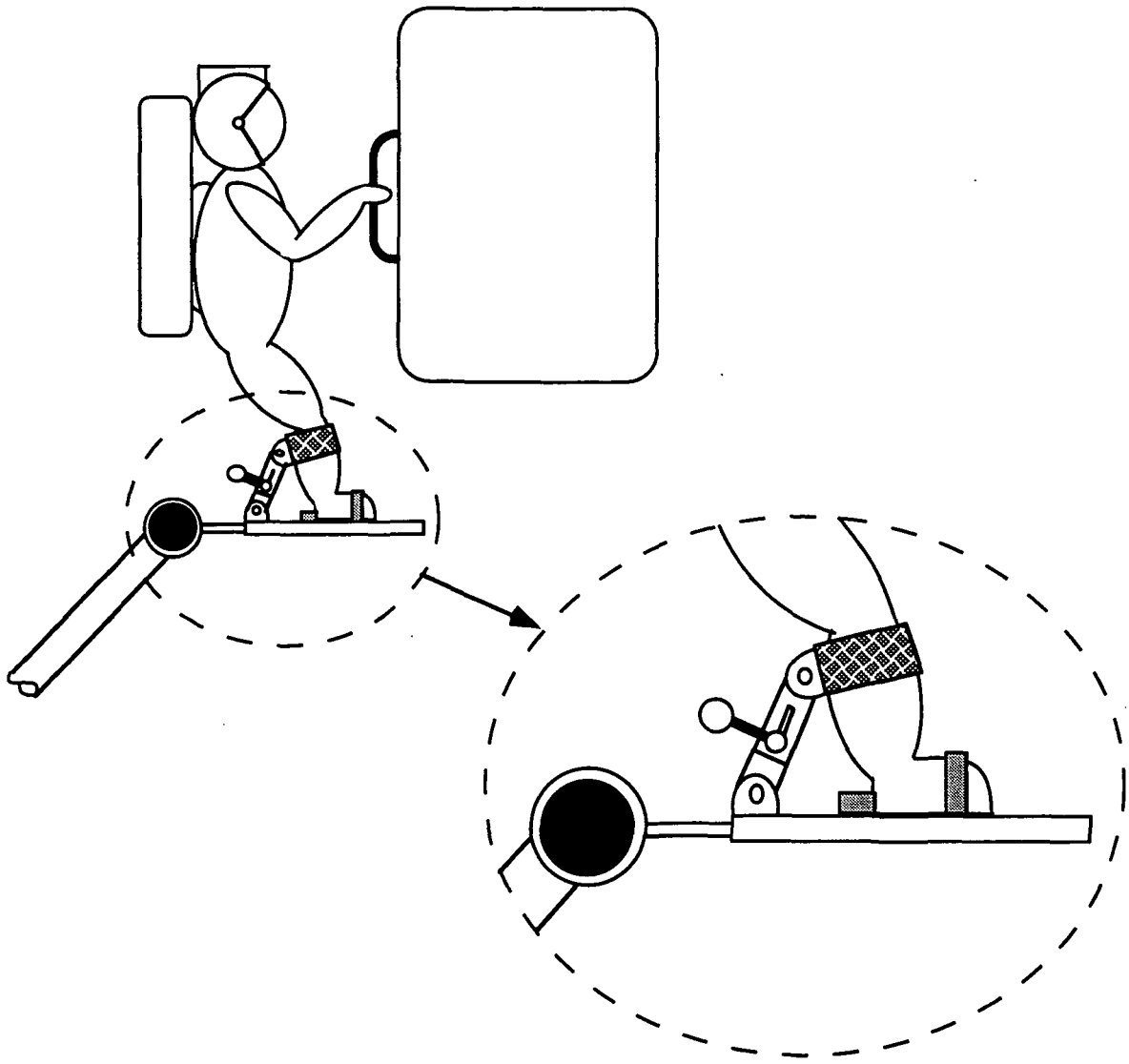

Figure 4.1 Lower leg brace device for reducing ankle torques during EVA mass manipulation tasks.

Although the work of creating the basic EVA dynamic simulation tool has progressed a great deal, there remain many future research activities to pursue; some of which are presented in the next section.

4.5 Recommended Future Research

The most obvious enhancements to the capabilities of the EVA dynamics simulation tool and some research questions to be addressed are summarized below. Greater accuracy of numerical results can be obtained by incorporating more precise data on the mass properties (segment mass, moments of inertia, and products of inertia) of human body segments. This data should be calculated as a function of the overall mass and

dimensions of the human subject being modeled. In addition, more realistic spring and damping constants should be obtained. It would also be helpful to include joint velocity limit curves and joint torque limits not already included.

One of the most important and novel contributions to the multibody system model of the human, in the case of EVA applications, would be the inclusion of the mechanical effects of the spacesuit on astronaut motions. It is anticipated that these effects can be largely modeled by the inclusion of torsional springs in the model's joints and by adding the space suit mass properties to the existing human body segment mass properties. The spacesuit model springs, which would act in parallel with other springs representing the passive and active torques of the human body itself, will likely require nonlinear equation forms to represent them. Furthermore, fabric suits usually exhibit a hysteresis pattern for joint torques that could be modeled. A qualitative sketch of a typical spacesuit joint torque curve is shown in Figure 4.2. There is great difficulty in finding published data on spacesuit joint torques. New experiments to measure spacesuit performance directly and establish data sets or regression equations for predicting joint torque based on position, direction of motion, and perhaps velocity may be necessary.

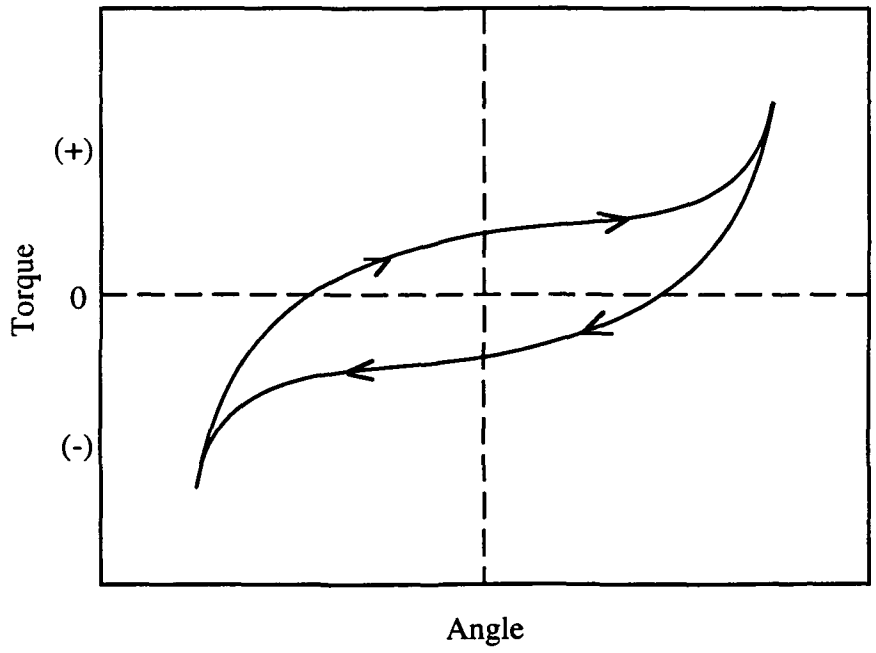

Figure 4.2 Typical spacesuit joint torque curve showing hysteresis effect.

The simulations described in this report are restricted to planar motion. It would be very interesting to provide the astronaut model with additional degrees of freedom (e.g., wrist flexion/extension and shoulder adduction/abduction) to enable three-dimensional

motions. The goal of a mass handling task, for instance, would be extended to following a three-dimensional trajectory. One should bear in mind, however, that adding degrees of freedom adds more variables to be evaluated or controlled and the added complexity may make it more difficult to interpret results or control the motion.

Another interesting topic to be investigated is the modeling of the dynamics of the Portable Foot Restraint (PFR), the Remote Manipulator System (RMS), and the Shuttle Orbiter as they relate to EVA tasks. Apparently there is already interest in this issue from NASA EVA training personnel and astronauts. As a first approximation, the Orbiter could be modeled as a single rigid body, the RMS as a three-link multibody system and the PFR as a single link attached to the RMS via a revolute joint with stiff springs.

An issue which needs to be studied further is that of multiple dynamic state solutions to systems with redundant degrees of freedom. In this research effort, solutions have been found by performing a linearized least squares operation. In the future, however, it may be more realistic to find solutions based on some sort of optimization, for instance minimum energy required.

The EVA tasks performed in the two simulations described in this report are specified directly by means of computer code. It would be of great use to alter the simulation code so that tasks (e.g., trajectory following, endpoint force exertion, etc.) can be specified through the graphical user interface environment provided by EVADS. This objective falls under the general goal of integrating the simulation code and EVADS program. It would also be worthwhile to develop algorithms that provide spline fits to keypoint trajectory or force data to avoid the user having to specify the EVA task in excessive detail.

An interesting extension of the simulation abilities would be to apply physiological analysis to the data obtained from the dynamical analysis. Kinematic and torque data could theoretically be used to calculate estimates of power, workload, and body temperature (for suit thermal regulation issues). Furthermore, employing physiological formulas might make it possible to estimate metabolic parameters such as O_2 uptake, CO_2 production, heart rate, cardiac output, and so on.

Up to now the control strategies applied in these EVA simulations have been quite rudimentary. An effort should be made to model human control strategies, such as optimal control or the McRuer crossover model (McRuer, Graham et al. 1965), and to include white noise and time delays in the human system.

Finally, but perhaps most importantly, there is a need to perform experimental verification of the simulation results. To mimic weightlessness, experiments could be performed in a neutral buoyancy facility or on a "zero-g" aircraft. Parabolic flight is less

likely to be used for these experiments due to the short duration of continuous weightlessness available (20-25 sec), particularly if the test subject is encumbered by a space suit. Whatever the facility, test subjects will perform mass manipulation of an object along a prescribed trajectory (probably aided by visual cues) while wearing a spacesuit. Tests should be conducted with the subject unsuited as well. The kinematics of the subject's motions (i.e., body segment positions, velocities, and accelerations) will be recorded by some means, for instance a video scan system picking up markers on the subject's spacesuit or body. Alternatively, there may be a possibility of employing a mechanical body motion measurement device, such as those manufactured by the EXOS company in Massachusetts. Unfortunately, there is no practical way of directly measuring the torque in the subject's joints (surgically implanted strain gages attached directly to tendons have been used on animals, but this is not a favored option for human subjects). Instead, the torques can be calculated from the kinematics data using inverse dynamics. Even though the torques themselves cannot be obtained by experiment directly, it is believed that kinematic data will sufficiently characterize the differences and similarities between the theoretical simulation results and the experimental results.

4.6 Summary Paragraph

This preliminary research effort has shown that the application of computational multibody dynamic simulations to extravehicular activity holds great promise as a valuable tool for analysts, trainers, and astronauts. For the first time, it is possible to obtain accurate numerical predictions of quantities such as joint angles and joint torques that are experienced in motion tasks, such as mass manipulation, tool handling, or translation and orientation of an astronaut's body, carried out during extravehicular activity. Having access to this quantitative information, combined with the qualitative information displayed in three-dimensional rendered graphics animation, enables the user to access important factors such as range of motion, exertion, and efficiency and comfort levels. In addition, it has been shown that computational simulation avoids many of the limitations of physical simulators, such as lack of degrees of freedom or friction, and is restricted only by the degree to which the user is willing or able to mathematically describe the physical principles and control laws involved. Furthermore, the convenience, low cost, and quick turnaround time of computational simulations greatly facilitates the process of exploring different scenarios for an EVA task and determining the optimum way in which to perform the desired procedure.

References

Armstrong, W. W. and M. W. Green (1985). "The dynamics of articulated rigid bodies for the purposes of animation." The Visual Computer **1**(4): 231-240.

Asada, H. and J.-J. E. Slotine (1986). Robot Analysis and Control. John Wiley and Sons.

Calderale, P. M. and G. Scelfo (1987). "Mathematical models of musculo-skeletal systems." Engineering in Medicine **16**(3): 131-146.

Cavagna, G. A., A. Zamboni, et al. (1972). "Jumping on the Moon: Power Output at Different Gravity Values." Aerospace Medicine (April): 408-414.

Chace, M. A. (1978). "Using DRAM and ADAMS Programs to Simulate Machinery, Vehicles." Agricultural Engineering (Nov, Dec): 18-19, 16-18.

Davis, B. L. and P. R. Cavanagh (1993). "Simulating reduced gravity: a review of biomechanical issues pertaining to human locomotion." Aviat. Space Environ. Med. **64**(June): 557-66.

Featherstone, R. (1983). "The Calculation of Robot Dynamics Using Articulated-Body Inertias." The International Journal of Robotics Research **2**(1): 13-30.

Fleischer, G. E. and P. W. Likins (1974). Attitude Dynamics Simulation Subroutines for Systems of Hinge-Connected Rigid Bodies. Jet Propulsion Laboratory.

Frisch, H. P. (1974). A Vector-Dyadic Development of the Equations of Motion for N Coupled Rigid Bodies and Point Masses. NASA.

Frisch, H. P. (1975). A Vector-Dyadic Development of the Equations of Motion for N Coupled Flexible Bodies and Point Masses. NASA.

Griffin, M. D. and J. R. French (1991). Space Vehicle Design. Washington, DC, AIAA.

Harwood, W. (1995). Spacewalk Estimate To Build Station Soars. SPACE NEWS. 4, 21.

Haug, E. J. (1989). Computer Aided Kinematics and Dynamics of Mechanical Systems - Volume 1: Basic Methods. Needham Heights, MA USA, Allyn and Bacon.

He, J., R. Kram, et al. (1991). "Mechanics of running under simulated low gravity." J. Appl. Physiol. **71**(3): 000-000.

Hemami, H. (1985). "Modeling, Control, and Simulation of Human Movement." CRC Critical Reviews in Biomedical Engineering **13**(1): 1-34.

Hollars, M. G., D. E. Rosenthal, et al. (1994). SD/FAST User's Manual. Symbolic Dynamics, Inc.

Holloway, T. W. (1992). INTELSAT Capture Lessons Learned. NASA.

Hooker, W. W. (1970). "A Set of r Dynamical Attitude Equations for an Arbitrary n-Body Satellite Having r Rotational Degrees of Freedom." AIAA Journal **8**(July): 1205-1207.

Hooker, W. W. (1974). Equations of Motion for Interconnected Rigid and Elastic Bodies: A Derivation Independent of Angular Momentum. Lockheed Missiles and Space Co.

Hooker, W. W. and G. Margulies (1965). "The Dynamical Attitude Equations for an n-Body Satellite." The Journal of the Astronautical Sciences **XII**(4): 123-128.

Isaacs, P. M. and M. F. Cohen (1987). "Controlling Dynamic Simulations with Kinematic Constraints, Behavior Functions, and Inverse Dynamics." Computer Graphics **21**(4, July): 215-224.

Isaacs, P. M. and M. F. Cohen (1988). "Mixed methods for complex kinematic constraints in dynamic figure animation." The Visual Computer **4**: 296-305.

Kane, T. R. and D. A. Levinson (1983). "Multibody Dynamics." Journal of Applied Mechanics **50**(December): 1071-1078.

Kane, T. R. and D. A. Levinson (1983). "The Use of Kane's Dynamical Equations in Robotics." The International Journal of Robotics Research **2**(3): 3-21.

Kane, T. R. and D. A. Levinson (1985). DYNAMICS: Theory and Applications. McGraw-Hill, Inc.

Kane, T. R., P. W. Likins, et al. (1983). Spacecraft Dynamics. New York, McGraw-Hill.

Kinzel, G. L. and L. J. Gutkowski (1983). "Joint Models, Degrees of Freedom, and Anatomical Motion Measurements." Journal of Biomechanical Engineering **105**(February): 55-62.

Kozloski, L. D. (1994). U.S. Space Gear : outfitting the astronaut. Smithsonian Institution.

Marshall, R. N., R. K. Jensen, et al. (1984). "A General Newtonian Simulation of an N-Segment Open Chain Model." Journal of Biomechanics **18**(5): 359-367.

McDonnell-Douglas (1994). The McDonnell Douglas Human Modeling System MDHMS Version 2.2.

McMahon, T. A. (1984). Muscles, Reflexes, and Locomotion. Princeton, NJ, Princeton University Press.

McRuer, D. T., G. Graham, et al. (1965). Human pilot dynamics in compensatory systems - theory, models and experiments with controlled element and forcing function variations. Air Force Flight Dynamics Laboratory, Wright-Patterson AFB, Ohio.

NASA (1987). Man-Systems Integration Standards.

NASA (1992). Space Shuttle Mission STS-49 Press Kit, Maiden Voyage of Endeavour.

Newman, D. J. and H. L. Alexander (1991). Human locomotion and workload for simulated lunar and martian environments. 42nd Congress of the International Astronautical Federation, Montreal, Canada, International Astronautical Federation.

Newman, D. J. and M. Barratt (1995). Chapter 22: Life Support and Performance Issues for Extravehicular Activity (EVA). Introduction to Space Life Sciences. Kleger Press, Orion Books (now in press).

Pandy, M. G., F. E. Zajac, et al. (1990). "An Optimal Control Model for Maximum-Height Human Jumping." J. Biomechanics **23**(12): 1185-1198.

Pandya, A. K., S. M. Hasson, et al. (1992). Correlation and Prediction of Dynamic Human Isolated Joint Strength From Lean Body Mass. NASA.

Pandya, A. K., J. C. Maida, et al. (1992). The Validation of a Human Force Model To Predict Dynamic Forces Resulting From Multi-Joint Motions. NASA.

Price, L. R., M. A. Fruhwirth, et al. (1994). Computer Aided Design and Graphics Techniques for EVA Analysis. 24th International Conference on Environmental Systems and 5th European Symposium on Space Environmental Control Systems, Friedrichshafen, Germany, Society of Automotive Engineers, Inc.

Ramey, M. R. and A. T. Yang (1980). "A Simulation Procedure for Human Motion Studies." Journal of Biomechanics **14**(4): 203213.

Reinhardt, A. (1989). Results and Applications of a Space Suit Range-of-Motion Study. 19th Intersociety Conference on Enviromental Systems, San Diego, CA, Society of Automotive Engineers, Inc.

Roberson, R. E. and J. Wittenburg (1966). A Dynamical Formalism for an Arbitrary Number of Interconnected Rigid Bodies, With Reference to the Problem of Satellite Attitude Control. The Third Congress of the International Federation of Automatic Control, London,

Rosenthal, D. E. and M. A. Sherman (1986). "High Performance Multibody Simulations via Symbolic Equation Manipulation and Kane's Method." The Journal of the Astronautical Sciences **34**(3, July-September): 223-239.

Schaechter, D. B. and D. A. Levinson (1988). Interactive Computerized Symbolic Dynamics for the Dynamicist. 1988 American Control Conference, Atlanta, GA USA, American Automatic Control Council (IEEE).

Scher, M. P. and J. R. Kane (1969). Alteration of the state of motion of a human being in free fall. Stanford University, Division of Applied Mechanics.

Silver, W. M. (1982). "On the Equivalence of Lagrangian and Newton-Euler Dynamics for Manipulators." The International Journal of Robotics Research **1**(2): 60-70.

Singh, R. P. and R. J. Vandervoort (1985). "Dynamics of Flexible Bodies in Tree Topology/a Computer-Oriented Approach." Journal of Guidance, Control and Dynamics **8**(5):

Steiner, M. D. and C. H. Seaman (1994). Extravehicular Activity Annex - Spartan 204. NASA.

Walker, M. W. and D. E. Orin (1982). "Efficient Dynamic Computer Simulation of Robotic Mechanisms." Journal of Dynamic Systems, Measurement, and Control **104**(September): 205-211.

Webbon, B. (1994). Human Requirements for Life Support and Extravehicular Activity in Space. Ames Research Center, NASA.

Wilhelms, J., M. Moore, et al. (1988). "Dynamic animation: interaction and control." The Visual Computer **4**: 283-295.

Wittenburg, J. (1979). The Dynamics of the Human Body. The Fifth World Congress on Theory of Machines and Mechanisms, ASME.

Wortz, E. C. and E. J. Prescott (1966). "Effects of Subgravity Traction Simulation on the Energy Costs of Walking." Aerospace Medicine (December): 1217-1222.